

Navigating uncertainty: reward location variability induces reorganization of hippocampal spatial representations

Charline Tessereau^{1*†}, Feng Xuan^{2*†}, Jack, R. Mellor^{3*‡}, Peter Dayan^{1,4*‡}
and Daniel Dombeck^{2*‡}

¹Max Planck Institute for Biological Cybernetics, Tübingen, Germany.

²Department of Neurobiology, Northwestern University, Evanston, Illinois, USA.

³School of Physiology, Pharmacology and Neuroscience, University of Bristol, Bristol, UK.

⁴University of Tübingen, Tübingen, Germany.

⁹*Corresponding author(s). E-mail(s): tessereau.charline@gmail.com;
¹⁰feng.xuan@northwestern.edu; Jack.Mellor@Bristol.ac.uk; dayan@tue.mpg.de;
¹¹d-dombeck@northwestern.edu;

¹²†These authors contributed equally to this work.

¹³‡These authors contributed equally to this work.

Abstract

Navigating uncertainty is crucial for survival, with the location and availability of reward varying in different and unsignalled ways. Hippocampal place cell populations over-represent salient locations in an animal's environment, including those associated with rewards; however, how the spatial uncertainties impact the cognitive map is unclear. We report a virtual spatial navigation task designed to test the impact of different levels and types of uncertainty about reward on place cell populations. When the reward location changed on a trial-by-trial basis, inducing expected uncertainty, a greater proportion of place cells followed along, and the reward and the track end became anchors of a warped spatial metric. When the reward location then unexpectedly moved, the fraction of reward place cells that followed was greater when starting from a state of expected, compared to low, uncertainty. Overall, we show that different forms of potentially interacting uncertainty generate remapping in parallel, task-relevant, reference frames.

Keywords: expected uncertainty, unexpected uncertainty, hippocampus, remapping, reward place cells

27 Introduction

28 Animals, including humans, thrive according to their ability to adapt to tasks, situations, and environments which vary in their regularity and associated uncertainties. For instance, while driving, minor unpredictable delays are common, would not prompt a route change and may even be unnoticed. They can thus be considered a form of *expected uncertainty* (often associated with aleatoric uncertainty or risk; Hüllermeier and Waegeman, 2021), in which precise outcomes are not fully foreseeable. However, a traffic jam can seem very surprising for someone used to a clear commute, a form of *unexpected uncertainty* (Soltani and Izquierdo, 2019; Yu and Dayan, 2005). This can indicate a significant contextual change that might necessitate significant adaptation, for instance, the need to use another route. Importantly, the threshold to consider an outcome as unexpected differs depending on expected uncertainty, for example, sporadic traffic jams might be customary to someone living in a busy capital, but prompting unexpected uncertainty in a small countryside town. For the brain to process and interpret these interacting forms of uncertainty is critical for adaptive behavior.

40 Most research on neural correlates of uncertainties has concentrated on aspects of decision-making, related to rewards and punishments (Behrens et al, 2007; Cohen et al, 2015; Dayan, 2012; Hsu et al, 2005; McGuire et al, 2014; Nassar et al, 2019; Preuschoff et al, 2011; Soltani and Izquierdo, 2019; Yu and Dayan, 2005). By contrast, it has rarely been applied to spatial contexts such as the location-specific traffic example above. In particular, the concept of uncertainty has not previously been applied to the description and understanding of spatial representations in the hippocampus and related structures, such as the well-studied place cells (Bast et al, 2009; Best et al, 2001; Burgess et al, 1995; Dombeck et al, 2010; Kleinknecht et al, 2012; Morris et al, 1990; Moser et al, 2008; Muller, 1996; O'Keefe and Dostrovsky, 1971; Radvansky et al, 2021; Sosa and Giocomo, 2021; Tessereau et al, 2021)(O'Keefe and Dostrovsky, 1971), even though many previous results might fit into such a general framework. For example, whether the hippocampal place cell population (i.e. the cognitive map) changes gradually or suddenly during a progressive change to the features (e.g. shape) of an animal's environment depends on the amount of experience the animal has had with the intermediate features (Leutgeb et al, 2005a; Plitt and Giocomo, 2021; Wills et al, 2005): the more experience, the more expected uncertainty and the more gradually the place cell population changes; the less experience, the less expected uncertainty and the more suddenly the place cell population changes. Though previous hippocampal research did not explicitly describe results in terms of uncertainty, insights for understanding how place cell populations might map environments with different levels of uncertainty can still be deduced.

58 In the case of expected uncertainty, for example, varying the spatial environment on a trial-by-trial basis (i.e., expected uncertainty in the spatial reference frame) caused hippocampal activity to reflect the statistics of the episodic environment (Plitt and Giocomo, 2021). Perhaps similarly, switching a stable reward location by block (e.g. expected uncertainty in reward location on a timescale of tens of minutes timescale) induces the progressive recruitment of reward-centred place cells (Gauthier and Tank, 2018; Issa et al, 2024; Sosa et al, 2023). However, reward foraging behaviors in nature often involve rapid, non-random, changes in reward locations in a stable spatial environment, a condition of expected uncertainty that has not been explored in prior studies. Therefore, it is unclear how the hippocampal place cell population encodes expected uncertainty in reward location on a trial by trial basis, independent of changes to the spatial reference frame.

68 In the case of unexpected uncertainty, numerous prior studies provide insights into how place cell populations change their encoding when animals are exposed to large, unexpected changes to their environments. This is typically induced by switching the animals to a novel arena or track which bears little resemblance to previously experienced spaces. These manipulations often result in a phenomenon known as remapping (Anderson and Jeffery, 2003; Bostock et al, 1991; Kentros et al, 1998; Leutgeb et al, 2005b; Muller and Kubie, 1987; Sanders et al, 2020), where place fields change their activity patterns between the two environments (Frank et al, 2004; Hill, 1978; Michon et al, 2021; Sheffield et al, 2017; Wills et al, 2005). While such "remapping" experiments are typically performed by changing aspects of space, prior studies have not looked at unexpected uncertainty in reward location, independent of changes to the spatial reference frame, without prior experience for such a move. Furthermore, in prior "remapping" experiments,

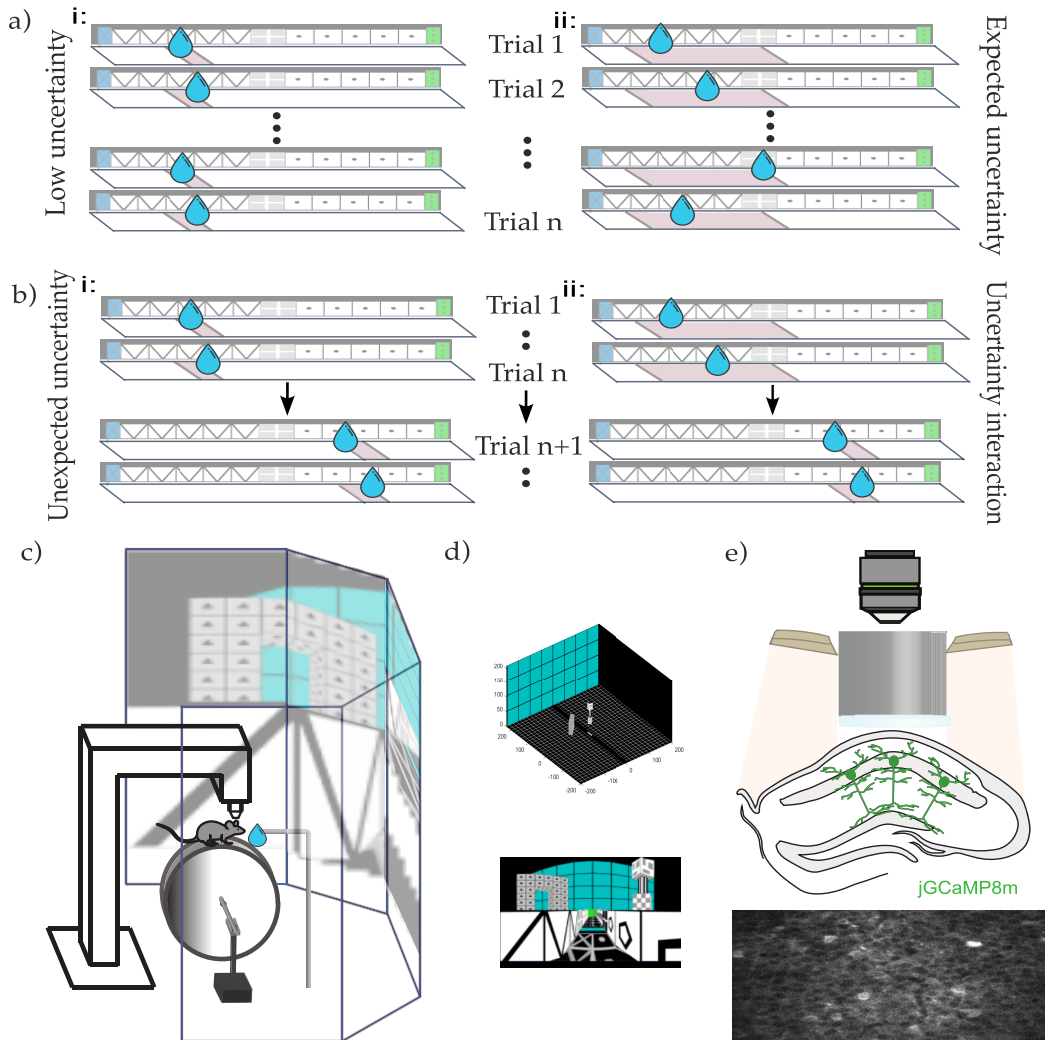
78 the level of uncertainty between the familiar and novel experiences has not been systematically varied.
79 Thus, not only is it not clear how changes to hippocampal representations in the light of unexpected and
80 expected uncertainty compare, but it is also unknown whether the encoding changes to place cells that
81 are induced by unexpected uncertainty depend on the initial level of expected uncertainty—that is, how
82 uncertainty interactions influence place cell mapping of environments.

83 To examine the consequences of uncertainties, we built a virtual reality spatial navigation task to test
84 explicitly the impact of different levels, types, and interactions of variability on the cognitive map. As
85 reward has been observed to be a particularly significant aspect of experience, potentially acting as an
86 anchor for cognitive maps (Burgess and O'Keefe, 1996; Dupret et al, 2010; Gauthier and Tank, 2018;
87 Jarzebowski et al, 2022; Sarel et al, 2017), we designed our task around uncertainty in the location
88 of reward. Mice were trained, in a stable spatial reference frame, to lick for a water reward whose
89 precise location on any trial was more or less certain (a form of expected uncertainty), and whose
90 location distribution might also translate without warning (unexpected uncertainty). During the task,
91 we imaged dorsal CA1 in the hippocampus using 2-photon calcium imaging (2P) (Dombeck et al, 2010)
92 of pyramidal cells expressing the calcium indicator jGCaMP8m (Zhang et al, 2023). We found that
93 expected uncertainty in reward location enhanced the proportion of place cells that tracked the reward
94 on a trial-by-trial basis compared to what we refer to as low uncertainty. Additionally, the reward and
95 the track end became anchors of a warped metric for space. Unexpected uncertainty caused substantial
96 remapping of place cells but, when we varied the initial level of expected uncertainty, we did not find a
97 difference in the overall proportion of place cells that remapped in the spatial reference frame. Instead,
98 starting from a state of high versus low expected uncertainty increased the proportion of reward and
99 warped place cells that moved to follow the reward after the unexpected change in reward location, a
100 condition that we termed uncertainty interaction. Starting from a state of low expected uncertainty, by
101 contrast, led to a less flexible representation in which reward location encoding place cells tended to
102 remain at the location of the initial reward, even after the unexpected change in reward location. Hence,
103 by inducing different forms of uncertainty in reward location and looking at their interaction, we show
104 that uncertainty generates remapping in parallel, task-relevant, reference frames.

105 Results

106 Mice adapt their behaviour to the degree of uncertainty of the task.

Fig. 1: Training protocol and imaging procedure



107 a) Training protocol: head-fixed mice on a wheel ran in 1d virtual reality (VR) environments in which water
108 reward was delivered at specific potential locations once per traversal of a 3m long linear track (and could subse-
109 quently be consumed anywhere by licking). In the low uncertainty condition (LU), the location could take one of
110 two positions at the edges of a 10cm reward zone (left). In the expected uncertainty condition (EU), there were 10
111 potential locations evenly spaced within a 90cm wide zone that were selected uniformly at random on every run
112 (right). Mice were trained on one session per day (on average $88.8 \text{ trials} \pm 15 \text{ std}$) until their behaviour was stable.
113 b) After training, mice experienced a switch session. Initial trials (on average $40.8 \pm 3.5 \text{ std}$) in the session
114 had the same location contingencies as those experienced during training. Without prior notice, the locations
115 at which reward might be provided switched to one of two positions at the edges of a more distal 10cm zone,
116 thus creating unexpected uncertainty (UU, left) in mice originally trained in LU, and a form of uncertainty
117 interaction (UI, right) for mice originally trained in EU.

- 118 c) Schematic of the VR apparatus: the licking behavior of mice was recorded as they ran on a wheel whose
119 turning determined the velocity of the visual flow on screens. When the mice reached the end of the track, the
120 screen went black for 3 seconds and mice were teleported to the start of the virtual track.
121 d) Visualization of the track used for VR in this paper. Top: 3D view of the track, showing the relative perspec-
122 tive with distal cues. Bottom: front view of the track.
123 e) Schematic of two photon calcium imaging of mouse CA1 neurons (green colors) expressing jGCaMP8m.
-
- 124
- 125

126 To study how different forms of reward location uncertainty affect the place cell code, we trained seven
127 male, water-scheduled mice to lick for a water reward as they ran on a 3m linear virtual reality (VR)
128 track, and simultaneously recorded place cell activity with 2-photon calcium imaging ([Dombeck et al,](#)
129 [2010](#)). At the end of the track, the screen switched off for 3 seconds and mice were teleported to the start
130 of the track for the next trial. On each trial, the reward location lay at discrete sites within a designated
131 reward zone of the track, with the width of this zone inducing varying degrees of predictability. In one
132 subgroup (3 mice, low uncertainty; LU), the reward was made available at one of two adjacent locations
133 10 cm apart, generating low (but, to avoid potential anomalies, not zero) uncertainty about the reward
134 location in each trial (Figure 1a:i). In the second group (4 mice, expected uncertainty; EU), the reward
135 was made available at one of ten potential locations within a 1-meter zone, creating a condition in which
136 mice could come to expect the resulting high aleatoric uncertainty (Figure 1a:ii). Importantly, the visual
137 environments were the same between the two groups, and contained extra-track cues, as well as a more
138 marked cue indicating the end of the track (Figure 1d). Once the mice were accustomed to the reward
139 contingencies in low or expected uncertainty conditions, they all experienced a switch in reward location
140 to a new, distal, 10 cm reward zone (Figure 1b). In the mice trained under LU, this switch induced a
141 form of unexpected uncertainty (UU, Figure 1b:i). In the mice trained under EU, this switch induced a
142 form of uncertainty interaction (UI, Figure 1b:ii).

143 Mice were first trained until they were accustomed to the specific reward contingencies of LU and EU.
144 Mice experiencing LU displayed licking and velocity patterns characteristic of high predictability: the
145 lick rate increased shortly before the reward zone, peaked within it, and then decreased, stopping until
146 the next trial (Figure 2a). These mice also slowed down as they approached the reward zone, stopped to
147 consume the reward, and then resumed running at a faster velocity until the end of the track (Figure 2a).

148 Mice trained in EU began licking and slowing down shortly before the start of the wider reward zone
149 (Figure 2b) and therefore appeared to treat the reward as occurring anywhere across the broad zone,
150 as expected for mice experiencing EU. To assess if the behavior in EU varied when the reward was
151 consumed at different locations in the reward zone, we averaged the licking and velocity profiles over
152 trials according to where the reward was consumed (see [Methods](#)) in the first third (proximal reward
153 trials; 146 in total), middle third (115 middle reward trials), and last third (111 distal reward trials) of
154 the reward zone. We found that mice licked persistently until they received the reward (Figure 2b). Once
155 they received the reward, mice ceased licking and began running in a stereotypical manner (similar to
156 LU; Figure 2b), demonstrating their understanding of the single-reward trial structure.

157 Hippocampal place cells organise into position, reward-centred, and warped 158 reference frames to reflect uncertainty

159 In order to investigate the population of place cells under these various conditions, we performed 2-
160 photon calcium imaging of dorsal CA1 pyramidal cells while mice performed the task. We extracted
161 place cells using an information theoretic criterion (see [Methods](#)), resulting in 1108 place cells for LU
162 and 1192 place cells for EU. We first confirmed that the LU condition of our task produced results that
163 were consistent with existing literature on place cell activity in reward navigation tasks by averaging
164 place cell activity (DF/F) over the recording session post-training in an external, position, reference
165 frame (Figure 2d:i). In the LU condition, we observed a higher density of place cells in the vicinity of the
166 reward zone (Figure ??:i), with on average 0.65% of cells per cm peaking in the vicinity of the reward

167 zone defined as being between 15 cm before, and 20 cm after, it (see [Methods](#)) -, against 0.26% elsewhere
168 (comparison in/out proportion z-test: p-value= 1.5×10^{-75} , comparison in>out 1-sided proportion z-
169 test: p-value< 7.3×10^{-76}). Place cells peaking in the vicinity of the reward zone had narrower place
170 fields (Figure ??:iii; comparison in/out t-test: p-value= 1.8×10^{-28} , comparison in<out 1-sided t-test:
171 p-value= 8.9×10^{-29}).

172 In the EU condition, we found only minor over-representation of the broad reward zone, with 0.35% of
173 place cells per cm peaking in the region between -15cm of the start, and +20cm of the end, of the zone
174 (see [Methods](#)), against 0.32% elsewhere (Figure ??:i, comparison in/out proportion z-test: $p = 1.3 \times 10^{-1}$,
175 EU comparison in>out 1-sided proportion z-test: $p = 6.6 \times 10^{-2}$). Place cells peaking in the vicinity
176 of the reward zone were also narrower in EU (Figure ??:iii ; comparison in/out t-test: $p = 1 \times 10^{-7}$,
177 comparison in>out 1-sided t-test: $p = 5.18 \times 10^{-8}$).

178 In this position reference frame, a higher proportion of cells was found to peak in the vicinity of the reward
179 zone in LU than EU (Figure ??:i; comparison LU/EU proportion z-test: $p = 7.9 \times 10^{-27}$, comparison
180 LU>EU 1-sided proportion z-test: $p = 4 \times 10^{-27}$).

181 To explore further the impact of a dynamically changing reward location on the place cell population
182 on a trial-by-trial basis, we compared the positions of peak activity for each cell between trials in which
183 the reward was collected near the start (proximal) or the end (distal) of the reward zone (scatter plots
184 in Figure 2f:i; quantification of stable neurons in Figure 2g, whose peaks are within the bounds shown
185 in Figure 2f:i). In the LU condition (Figure 2f:i; g:blue bar), in which these positions are very close,
186 73.10% of place cells maintained their peak activity location across the two groups of trials, compared
187 to only 41.19% under EU (Figure 2f:i; g:purple bar; proportion z-test between the percentages in LU
188 in EU: $p = 1 \times 10^{-53}$. 1-sided proportion z-test LU>EU $p = 5.26 \times 10^{-54}$). We also examined the
189 locations of the peaks of the place fields of these cells and found that position-stable cells are evenly
190 distributed, with 38.3% of those cells located before the reward zone for LU (c.f. 31.9% for EU), 27.9%
191 (c.f. 32.22% for EU) in the vicinity of the reward zone, and 33.8% (c.f. 35.93% for EU) after the reward
192 zone (Figure 2j). Although the total percentages are similar, the reward zone area is wider, and starts
193 earlier in the track, in EU, resulting in a higher relative proportion of cells per cm before the reward zone
194 (Figure 2k:i; comparison proportion z-test LU/EU $p = 3.47 \times 10^{-28}$, 1-sided proportion z-test LU<EU
195 $p = 4.41 \times 10^{-28}$) and lower in the vicinity of the reward zone compared to LU (Figure 2k:ii; comparison
196 proportion z-test LU/EU $p = 8.82 \times 10^{-28}$, 1-sided comparison z-test LU>EU $p = 4.41 \times 10^{-28}$).

197 Given that the reward changes location on a trial-by-trial basis, particularly in the EU condition, and
198 that place cells can become organised within different task-relevant reference frames with experience
199 (Anderson and Jeffery, 2003; Aoki et al, 2019; Gauthier and Tank, 2018; Markus et al, 1995; Muzzio
200 et al, 2009; Plitt and Giocomo, 2021; Radvansky et al, 2021; Sosa and Giocomo, 2021; Sosa et al, 2023),
201 specifically reward (Burgess and O'Keefe, 1996; Gauthier and Tank, 2018; Jarzebowski et al, 2022; Sosa
202 and Giocomo, 2021; Sosa et al, 2023), we asked whether the EU condition might reinforce the reward
203 reference frame, possibly reflected in an increased population representing the changing variable. We
204 therefore considered whether cells code for position *relative* to the reward location on a trial rather than
205 in spatial position associated with the track. To examine this we averaged cell activity relative to reward
206 position (Figures 2d:ii; e:ii, see [Methods](#)). In contrast to the position reference frame, in the reward
207 reference frame, there was an equal accumulation of cells aligned in the vicinity of the reward in both
208 LU and EU conditions (Figure ??:ii), with 4.8% of cells per cm in the vicinity of the reward (with a
209 peak of activity between -15cm and +20cm of the reward), against only 0.2% of cells per cm outside
210 these bounds, in LU (comparison in/out proportion z-test: p-value< 0.2×10^{-308} , comparison in>out
211 1-sided proportion z-test: p-value< 2.2×10^{-308}), and 3.4% per cm in the vicinity of the reward, against
212 1.25% per cm elsewhere in EU (comparison in/out proportion z-test: p-value< 2.2×10^{-308} , comparison
213 in>out 1-sided proportion z-test: p-value< 2.2×10^{-308} ; Figure ??:ii). Averaging in a reward-centered
214 reference frame also reduced the widths of place fields peaking in the vicinity of the reward compared to
215 elsewhere, for both LU (comparison in/out proportion z-test: p-value= 3.2×10^{-28} , comparison in<out
216 1-sided proportion z-test: p-value< 1.61×10^{-28}) and EU (comparison in/out proportion z-test: p-
217 value= 1.6×10^{-12} , comparison in<out 1-sided proportion z-test: p-value< 8.11×10^{-13} ; Figure ??:iv). The
218 difference in accumulation of reward place cells between position and reward reference frames revealed a

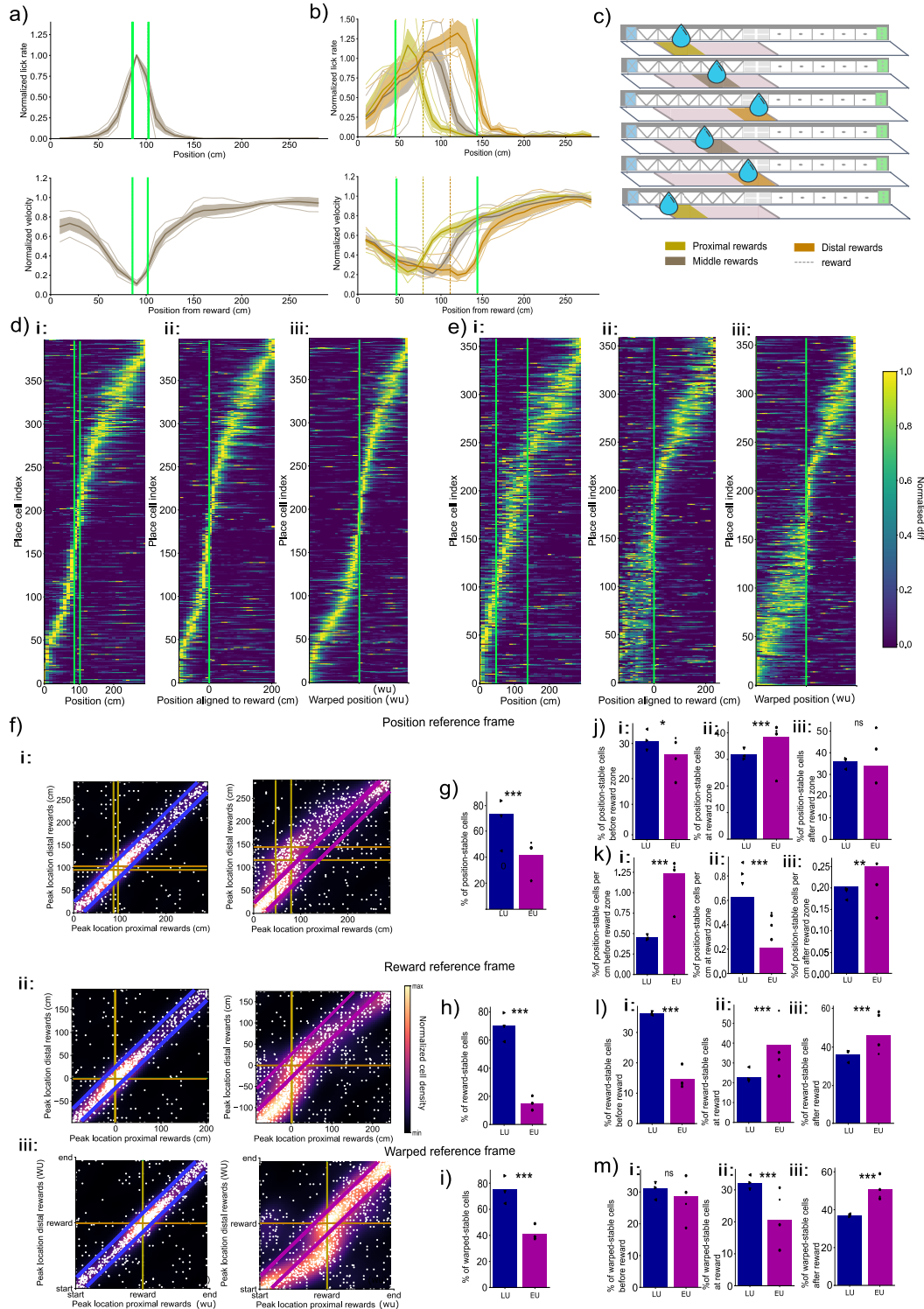
219 population of cells that stably followed the reward on every trial (termed reward cells) and was confirmed
220 by single-cell activity profiles across all trials (Figure ??), highlighting populations of cells with stable
221 fields relative to position and also reward. These reward cells generalize previous findings (Gauthier and
222 Tank, 2018) to our task in which the reward changes location on every trial.

223 To investigate the effect of a dynamically changing reward location on the place map in this reward
224 reference frame, we compared the locations of peak activity with respect to reward location between
225 proximal and distal reward trials. We found that 70.21% of the place cells maintained their peak activity
226 relative to the reward location across the two groups of trials in LU, compared with 14.85% in EU (Figure
227 2f:ii, with the stable neurons shown in the boxes quantified in Figure 2h; proportion z-test LU/EU:
228 $p = 1 \times 10^{-159}$, 1-sided proportion z-test LU>EU $p = 5.51 \times 10^{-160}$). Examining the distribution of these
229 cells along the track (Figure 2l), we found that 36.25% of the reward-stable cells were before the reward
230 in LU, compared to 14.69% in EU (Figure 2l:i; comparison proportion z-test $p = 3.06 \times 10^{-8}$, 1-sided
231 proportion LU>EU z-test $p = 1.53 \times 10^{-8}$). Stability of encoding at the reward was most enhanced in
232 EU, with 38.98% of reward-stable cells being located in its vicinity, compared to 22.87% of reward-stable
233 cells in LU (Figure 2l:ii; comparison LU/EU proportion z-test $p = 5.02 \times 10^{-5}$, 1-sided proportion z-test
234 LU<EU $p = 5.02 \times 10^{-6}$). After the reward, less stability was reported in LU, with 36.24% of reward-
235 stable cells compared to EU, with 46.33% of reward-stable cells (Figure 2l:iii; comparison proportion
236 z-test $p = 1.27 \times 10^{-2}$, 1-sided proportion z-test LU<EU $p = 6.34 \times 10^{-3}$).

237 While the reward location cannot be predicted, the part of each run from the reward to the end of the
238 track is predictable, and is characterized by a stereotypical behavioral routine. Hippocampal activities
239 have been shown to reflect the statistics of the episodic environments animals experience (Plitt and
240 Giocomo, 2021), for example reflecting stereotypical behavioural sequences (Skaggs and McNaughton,
241 1998), and organising along warped metrics that homogenise similar episodes (Gothard et al, 1996). We
242 therefore asked whether the hippocampus might similarly represent these post-reward events regardless
243 of reward location, reflecting stereotypical changes. Consistent with this idea, we qualitatively observed
244 a group of cells that seemed to span the range from the reward location to the end of the track in a
245 flexible manner (Figure 2f:i). To quantify this, we considered a third, warped, metric for space in which
246 we compressed and expanded it so that there were two segments of 20 bins each — one linking the start
247 of the track to the reward location and the other from the reward location to the end of the track (Figure
248 2d:iii; e:iii). We found that 75.4% of cells kept their position of peak activity in the warped reference
249 frame between proximal and distal reward trials in LU, and 41.1% in EU (Figure 2i). Examining the
250 relative distributions of warped-stable cells around the reward location in this reference frame, we found
251 a balanced distribution in LU: 31.01% of warped-stable cells before the reward, 32.0% in the vicinity of
252 the reward, and 36.8% after the reward (Figure 2m). As the reward location cannot be predicted in EU,
253 this analysis is provided here for completeness with respect to other reference frames. In contrast, the
254 warped metric highlighted a post-reward alignment of cells after the reward in EU, with 28.51% of the
255 warped-stable cells before the reward, 20.7% in the vicinity of the reward, and 50.7% after the reward.
256 We found a significantly lower degree of post-reward warping in LU compared to EU (Figure 2m:iii;
257 comparison proportion z-test $p = 8.40 \times 10^{-7}$, 1-sided proportion z-test LU<EU $p = 4.2 \times 10^{-7}$).

258 Note that the higher percentages of stability between proximal and distal reward trials reported in Figures
259 2g,h,i in low uncertainty simply reflect the task design, in which reward, position and warped reference
260 frames are more similar in LU than in EU due to its far narrower reward zone. We provide the statistical
261 comparisons for the sake of completeness. Our finding of excess stability in reward (Figure 2l) and warped
262 reference frames (Figure 2m) in EU confirm our conclusion that expected uncertainty highlights enhanced
263 reward and warped reference frames as an adaptation to reflect the statistics of change in the task
264 design. Overall, our findings show that expected uncertainty in reward location enhanced the proportion
265 of place cells that tracked the reward on a trial-by-trial basis (reward-referenced cells) compared to low
266 uncertainty, and the reward and the track end became anchors of a warped metric for space.

Fig. 2: Expected uncertainty reveals dual spatial and reward reference frames for behaviour and place cell activity, and a warped metric that combines both



267 a) i: Average lick rate (number of lick events per 10cm position bin) after training in the LU condition.
268 ii: Average velocity trace in the same condition. For both: Thick line shows the mean across sessions

269 ($n = 12$ sessions, $m = 3$ mice) normalised to the maximum per session, shaded region represents the
270 standard deviation across sessions; shaded lines show each session trace. iii;iv: The same plots as for
271 LU, but under EU, for laps of trials separated as shown in b): yellow: proximal, grey: middle and orange
272 distal reward trials. For both top and bottom: Thick line showing the mean across sessions ($n = 16$
273 sessions, $m = 4$ mice) normalised to the maximum per session, shaded region represents the std across
274 sessions, shaded lines show each session trace. Green thick lines show the reward zone.
275 b) Diagram of the division between the laps according to the location at which the reward was consumed
276 for the analysis in EU.
277 c) i: Cross validated place map in a position reference frame for one session of LU for one animal, showing
278 the average place cell activities ($N = 437$ place cells out of 518 total cells) on even trials normalised
279 to their maximum value, ordered by their position of peak activity on odd trials, after training in low
280 uncertainty. ii: The same activity, but averaged according to a reward reference frame (aligning the
281 position to the reward location at every trial – see [Methods](#)). iii: The same activity averaged according
282 to a warped/interpolated position-reward reference frame (a warped metric vector is created by two
283 uniform interpolations linking the start of the track - reward - end of the track – see [Methods](#)).
284 d) The same (c), but for an animal experiencing EU ($N = 369$ place cells out of 475 total cells).
285 e) i: Scatter plot showing the positions of peak activity on trials on which the reward is at the proximal
286 (x-axis) versus distal (y-axis) end of the reward zone for LU (left; 1118 place cells) and EU (right; 1192
287 place cells). Each white dot is a single place cell; the heatmaps show a probability density function esti-
288 mate of the data (see [Methods](#), normalised to 1). Yellow lines show the reward zone on proximal trials,
289 orange lines on distal trials. Blue lines (left) and purple lines (right) delineate the diagonal used in the
290 quantification for statistics in f). Scatter plots include a jitter proportional to cell density, enhancing
291 visualization of overlapping data points. ii: Similar to (i), but in a reward-centered reference frame. The
292 yellow line shows the reward location on proximal trials, the orange line on distal trials (both at 0, by
293 definition of the reward reference frame). Blue square (left) and purple square (right) delineate the area
294 used in the quantification for statistics in g). iii: similar to (i) in a warped metric (see [Methods](#)). Blue
295 lines (left) and purple lines (right) delineate the post-reward diagonal used in the quantification for
296 statistics in h).
297 f) Percentages of cells that have a similar ($\pm 15\text{cm}$) position of peak activity in ‘proximal’ and ‘dis-
298 tal’ reward trials in LU (blue region) and EU (purple region). comparison proportion z-test LU/EU
299 $p = 1 \times 10^{-53}$, 1-sided proportion z-test LU>EU $p = 5.26 \times 10^{-54}$.
300 g) Same than f) in a reward reference frame. Comparison proportion z-test LU/EU $p = 1.1 \times 10^{-159}$,
301 1-sided proportion z-test EU>LU $p = 5.51 \times 10^{-160}$.
302 h) Same than g) in a warped reference frame (± 3 warped units). Comparison proportion z-test LU/EU
303 $p = 1.2 \times 10^{-61}$, 1-sided proportion z-test EU>LU $p = 5.6 \times 10^{-62}$.
304 i) Percentages of cells that are stable in a position reference frame (with a maximum displacement
305 of $\pm 15\text{cm}$; within the diagonal lines in e:i): i: before the reward zone, comparison proportion z-test
306 $p = 1.77 \times 10^{-2}$, 1-sided proportion z-test LU<EU $p = 8.86 \times 10^{-3}$; ii: in the vicinity of the reward
307 zone ($-15 +20\text{cm}$), comparison proportion z-test $p = 8.82 \times 10^{-28}$, 1-sided proportion z-test LU>EU
308 $p = 4.41 \times 10^{-28}$, iii: after the reward zone, comparison proportion z-test $p = 3.17 \times 10^{-2}$, 1-sided
309 proportion z-test LU<EU $p = 1.59 \times 10^{-2}$, for LU (blue) and EU (purple).
310 j) Same as (i) but divided by the total area covered by every zone. left: comparison proportion z-test
311 $p = 3.47 \times 10^{-28}$, 1-sided proportion z-test LU<EU $p = 1.73 \times 10^{-28}$ middle: comparison proportion
312 z-test $p = 1.96 \times 10^{-10}$, 1-sided LU>EU comparison test $p = 5.31 \times 10^{-11}$, right: comparison proportion
313 z-test $p = 2 \times 10^{-1}$.
314 k) Percentages of cells with stable peaks in a reward reference frame ($\pm 15\text{cm}$; within the boxes in e:ii):
315 i: before the reward, comparison proportion z-test LU/EU $p = 3.06 \times 10^{-8}$, 1-sided proportion LU>EU
316 z-test $p = 1.53 \times 10^{-8}$. ii: in the vicinity of the reward zone ($[-15, +20]\text{cm}$), comparison LU/EU propor-
317 tion z-test $p = 1 \times 10^{-5}$, 1-sided proportion z-test LU<EU $p = 5.02 \times 10^{-6}$. iii: after the reward zone,
318 comparison proportion z-test $p = 1.27 \times 10^{-2}$, 1-sided proportion z-test LU<EU $p = 6.34 \times 10^{-3}$, for
319 LU (blue) and EU (purple).
320 l) Percentages of cells with stable peaks in a warped reference frame (with a maximum dis-
321 placement of 3 warped units, representing between 20cm and 40cm, depending on the position
322 of the reward; within the diagonal lines in e:iii): i: before the reward, comparison proportion
323 z-test LU/EU $p = 3.37 \times 10^{-1}$, non significant. ii: in the vicinity of the reward zone ($-2 +3$

324 warped units), comparison proportion z-test $p = 9.06 \times 10^{-6}$, 1-sided proportion LU>EU z-
325 test $p = 4.53 \times 10^{-6}$. iii: after the reward zone, for LU (blue) and EU (purple), comparison
326 proportion z-test LU/EU $p = 8.4 \times 10^{-7}$, 1-sided proportion LU<EU z-test $p = 4.2 \times 10^{-7}$.

327

328

329 **Expected uncertainty leads to enhanced flexibility of the reward and warped**
330 **populations towards a surprisingly new reward location.**

331 We have so far shown that expected uncertainty leads to an enhanced reward and warped reference
332 frame by contrasting with a condition of low uncertainty. To complement the collection of uncertainties,
333 and investigate their interaction, we performed a larger, unpredictable, change in reward location meant
334 to induce a sudden surprise and a condition of unexpected uncertainty. After familiarising the animals
335 to the LU and EU conditions, we imaged CA1 place cells while changing the reward location during a
336 session, without prior notice or experience, to a narrow reward zone further down the track (Figure 1b).
337 This unannounced change generates unexpected uncertainty (UU) in LU mice and a form of uncertainty
338 interaction (UI) in EU mice. As drastic changes in context can lead to very abrupt shifts in place field
339 locations (Michon et al, 2021; Sheffield et al, 2017; Wills et al, 2005), we asked whether UU would
340 induce a higher degree of change in the place map compared to UI, due to a higher level of surprise.
341 Comparison between LU and EU highlighted a difference with respect to the anchor of the reward on
342 the place map, but it was unclear if or how these differences would change the response to unexpected
343 uncertainty. Specifically, noting that the reward location variability in the EU mice led them to have a
344 greater proportion of place cells stably tied to reward and warped reference frames rather than position,
345 we tested whether this would generalize to the farther move of the reward, which would be exemplified
346 by greater stability in these reference frames for UI than UU in the face of an unexpected change.

347 We first verified that the behavior after the switch stabilizes to a pattern reflecting the new task statistics.
348 The licking and velocity patterns aligned with prior observations (compare Figures 2a;b and 3a;b). Note
349 that the two subjects in UI had different patterns of post-switch behavior (Figure ??); thus, as well as
350 analyzing them together we report in the Supplement (Figures S?? and S??) the statistical comparisons
351 presented in this section for each of these animals separately.

352 Next, we examined how the place map was impacted by the unexpected change. Although we expected
353 more global remapping in UU than UI (since they should have been more surprised), a qualitative
354 assessment of the place map after the switch (Figure 3c;d) highlighted similar, moderate, degrees of
355 remapping in both conditions, primarily affecting place cells peaking between the previous and new
356 reward zones. Comparing post-switch maps, we found that reward over-representation was marginally
357 less in the new location under UU than UI. Indeed, after UU we found 0.38% of cells per cm in the vicinity
358 of the reward after UI and 0.28% of cells per cm elsewhere (proportion z-test UU/UI $p = 1.13 \times 10^{-2}$,
359 1-sided z-test UU<UI $p = 5.6 \times 10^{-3}$, Figure ??).

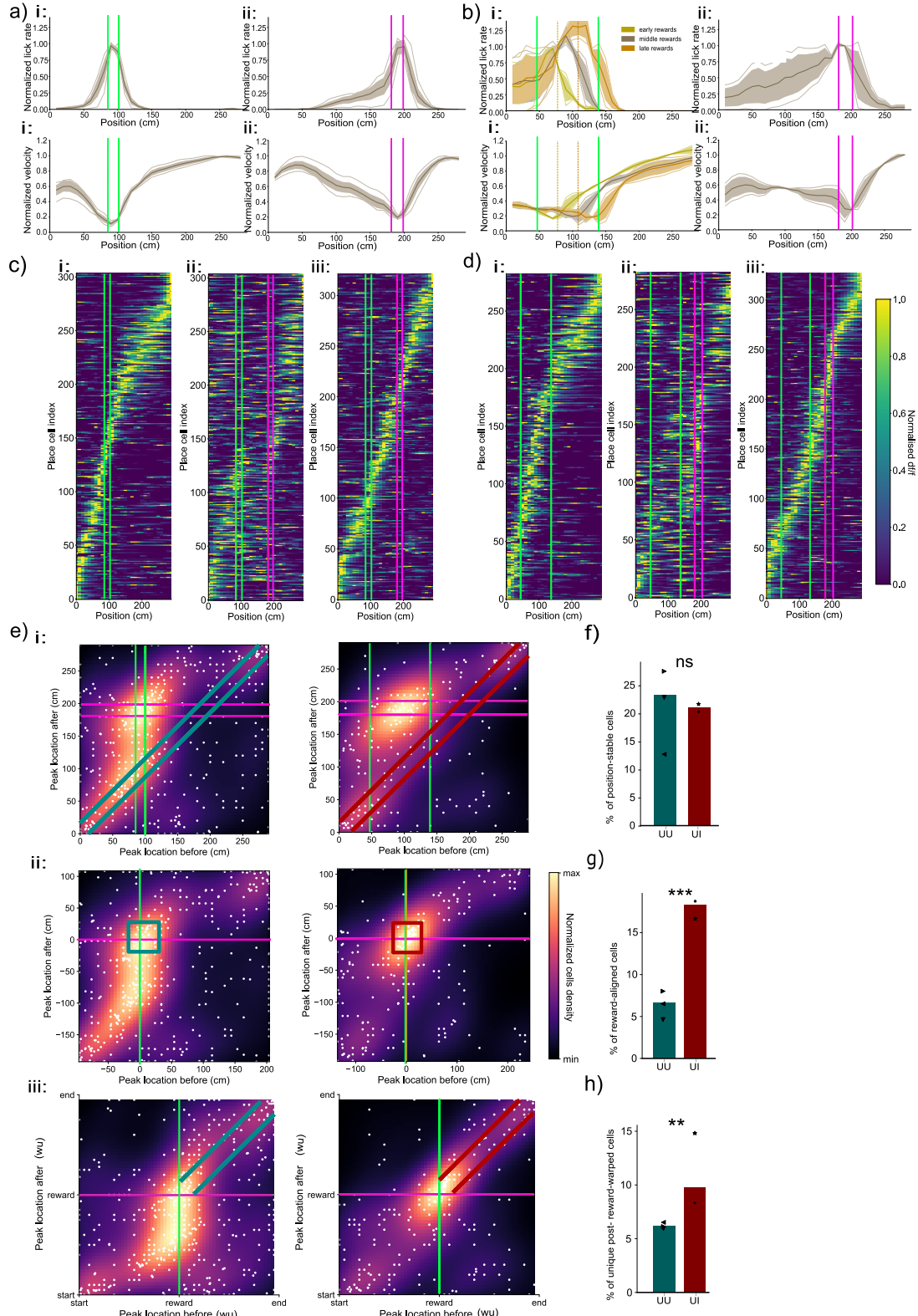
360
361 To quantify the impact of the sudden reward location change on each place cell's activity, we compared
362 the location of peak activity before and after the switch for cells that remained place cells after the
363 switch (455 place cells out of 1872 total cells for UU, 246 out of 970 for UI). Surprisingly and contrarily
364 to our expectations, we found that similar percentages of cells maintained their peak activity location
365 after the switch in UU (24.4% of cells) and UI (21.5% of cells) in a position reference frame (Figure 3e;h;
366 comparison proportion z-test UU/UI $p = 4 \times 10^{-1}$). Thus, unexpected uncertainty caused substantial
367 remapping of place cells but, when we varied the initial level of expected uncertainty, we did not find a
368 difference in the overall proportion of place cells that remapped in the spatial reference frame.

369 However, building on the observation of a slightly lower reward over-representation after UU compared
370 to UI, we turned to analyse the cells that moved with the reward across the switch in a reward reference
371 frame. We found that a significantly lower percentage of cells stably peaked in the vicinity of the reward
372 in a reward-reference frame across the switch in UU (7% of cells) than in UI (18.2% of cells) (Figure 3f;i;

373 comparison proportion z-test UU/UI $p = 1.73 \times 10^{-6}$, 1-sided proportion z-test UU<UI $p = 8.65 \times 10^{-7}$),
374 excluding those place cells that were stable in the position reference frame (i.e., those quantified in Figure
375 3h). Thus, expected uncertainty leads to a more flexible reward reference frame.

376 We then wondered whether the enhanced flexibility of the reward anchor in UI would also translate
377 to the warped reference frame. Indeed, we found that fewer cells maintained their peak activity in UU
378 (6% of cells) compared to UI (14% of cells) in the warped reference frame (Figures 3g;j; comparison
379 proportion z-test UU/UI $p = 2.94 \times 10^{-3}$, 1-sided proportion z-test UU<UI $p = 1.47 \times 10^{-3}$), excluding
380 any position-stable or reward-peaking cells quantified in Figures 3h;i. Therefore, expected uncertainty
381 leads to hippocampal representations that are more stable in both the reward and warped reference
382 frames in subsequent adaptations to unexpected changes.

Fig. 3: Expected uncertainty in reward location enhances flexible reward and warped reference frames



383 a) UU: Top: normalized lick rate averaged over all sessions. i: before the switch, ii: after the switch.
384 Bottom: similar to Top) for normalized velocity. Green thick lines show the full reward zone. Shaded
385 areas show standard deviations and individual lines show individual sessions averages.
386 b) UI: Top: normalized lick rate on proximal (Yellow), middle (Grey) and distal (Orange) reward trials.
387 i: before the switch, ii: after the switch. Bottom: similar to Top) but for normalized velocity. Green thick
388 lines show the full reward zone before the switch, pink lines the reward zone after the switch. Shaded
389 areas show standard deviations and individual lines show individual sessions averages. See Figure ?? for
390 results for separate mice.
391 c) i: Place map before the switch (N place cells=304) in UU, showing the average activity for one ani-
392 mal, ordered according to their cross-validated position of peak activity before the switch, and shown in
393 a position reference frame. Green lines mark the reward zone. ii: activities of the same cells ordered as
394 in (i), after the switch. Turquoise lines mark the previous reward zone, pink lines show the new reward
395 zone. iii: New place map after the switch (N after=322).
396 d) The same as (c), but for UI (N before=283, N after=328).
397 e) i: Scatter plot showing the positions in a position reference frame of peak activity before (x-axis)
398 versus after the switch (y-axis) in UU (left) and UI (right). Each white dot is a cell and heatmap shows
399 a probability density function estimate (see [Methods](#)). Turquoise lines delineate the diagonal used for
400 statistics in f). Scatter plots include a jitter proportional to cell density, enhancing visualization of
401 overlapping data points. ii: Similar to i: but in a reward reference frame. Turquoise squares delineate
402 the area used for statistics in g). iii: Similar to (i;ii:) but in a warped reference frame. Turquoise lines
403 delineate the post-reward diagonal used for statistics in g).
404 f) Percentages of cells with stable peaks in a position reference frame (with a maximum displacement
405 of $\pm 15\text{cm}$; shown by the lines in the heatmap in e)i: : for UU (turquoise) and UI (red). The black dots
406 show individual session percentages. Comparison proportion z-test UU/UI $p = 5.14 \times 10^{-1}$.
407 g) Percentages of cells with stable peaks in a reward reference frame (between -15cm and $+20\text{cm}$ of
408 the reward; shown by the lines in the heatmap in e)ii:), excluding position-stable cells. Proportion z-test
409 UI/UU $p = 1.73 \times 10^{-6}$, 1-sided comparison UU<UI 1-sided proportion z-test $p = 8.65 \times 10^{-7}$.
410 h) Percentages of cells with stable peaks in a warped reference frame (with a maximum displacement
411 of 3 warped units, representing between 20cm and 40cm, depending on the position of the reward,
412 shown by the lines on the heatmaps in e)iii:), excluding position- and reward-stable cells. Proportion
413 z-test UU/UI $p = 2.94 \times 10^{-3}$, 1-sided comparison UU<UI 1-sided proportion z-test $p = 1.47 \times 10^{-3}$.

414

415

416 Place cells over-represent previous rewards in UU, generalize in UI

417 Surprised by the finding that the proportion of cells maintaining their peak activity location before
418 and after the switch was similar in UU and UI conditions in a position reference frame, we decided to
419 investigate further the relative stability in position reference frame, and looked at how the peaks of these
420 position-stable cells were distributed along the track. The distributions of percentage of cells per position
421 bin did not show any significant overall difference between the two conditions (Kolmogorov-Smirnov test
422 $p = 0.872$, non significant; figure 4a).
423 However, minor differences were apparent when dividing the track up into three areas: ahead of the reward
424 zone before the switch, at the previous reward zone, and the remainder (zones marked with bars in the
425 insert in Figure 4a). In UU, a slightly greater position-stability was observed before the previous reward
426 zone, with 11.87% of cells (50.5% of total position-stable cells) located before the previous reward zone
427 in UU, compared to 7.72% of cells (35.8% of total position-stable cells) in UI (Figure 4b:ii; comparison
428 UU/UI proportions z-test $p = 6 \times 10^{-2}$, 1-sided proportion z-test UU>UI $p = 2.27 \times 10^{-1}$). In the vicinity
429 of the previous reward zone, no significant difference was found, with 4.4% of cells (18% of position-
430 stable cells) in UU and 6.5% of cells (30% of position-stable cells) in UI (Figure 4b:iii; comparison UU/UI
431 proportions z-test $p = 2.2 \times 10^{-1}$, non significant). After the previous reward zone, a similar proportion
432 of cells was position-stable, with 7.7% of cells (31.5% of position-stable cells) in UU and 7.3% of cells

433 (34% of position-stable cells) in UI (Figure 4b:iv; comparison UU/UI proportions z-test $p = 8.6 \times 10^{-1}$,
434 non significant).

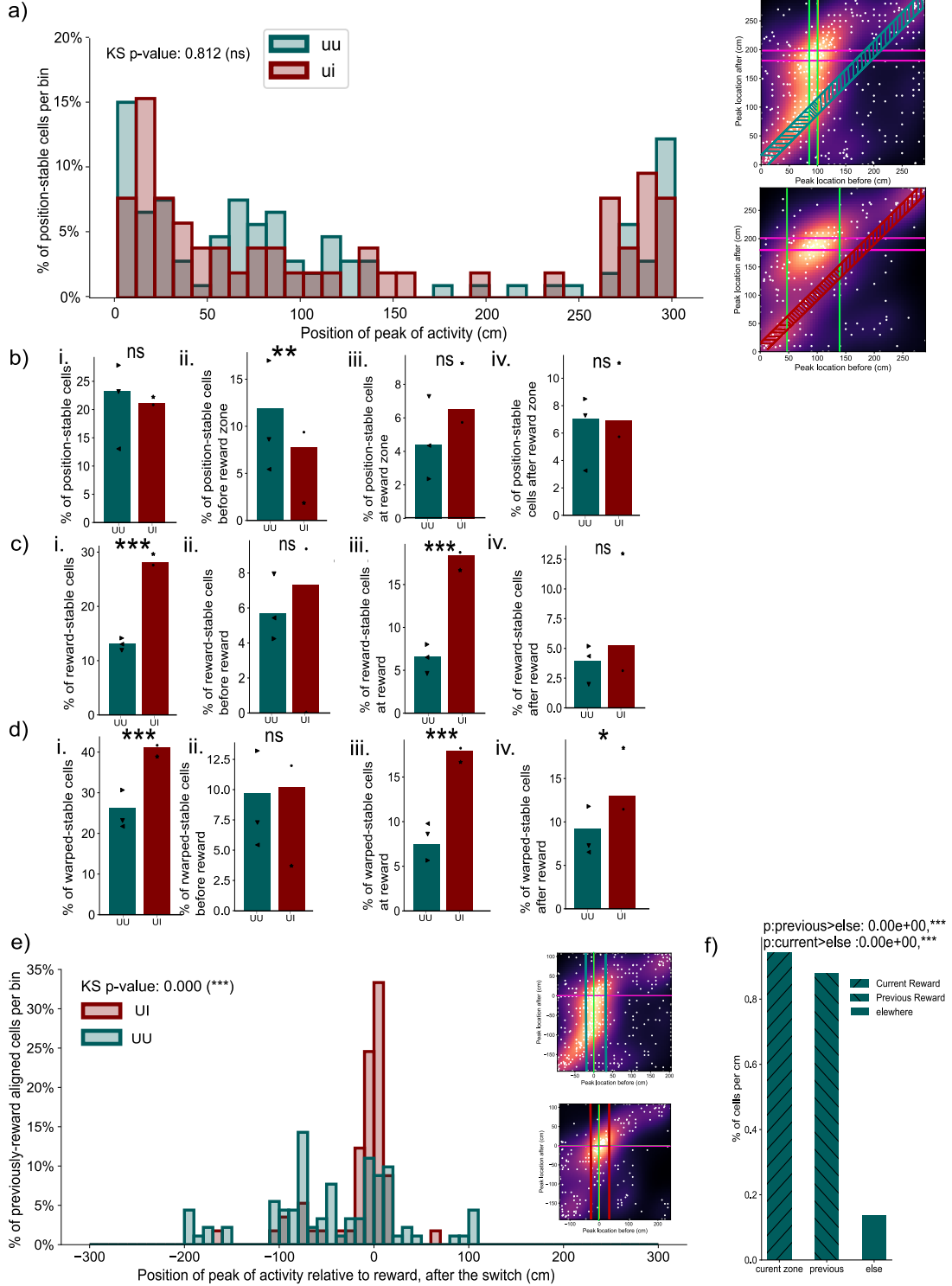
435 Consistent with our results so far, this picture changed considerably in a reward reference frame (Figure
436 4c). Here, we found greater overall reward-stability in UI, with only 13.6% of cells maintaining their
437 peak activity location relative to the reward after the switch in UU, compared to 28% of cells in UI
438 (Figure 4c:i; comparison UU/UI proportions z-test $p = 3 \times 10^{-6}$, comparison UU<UI 1-sided proportion
439 z-test $p = 2.7 \times 10^{-6}$). Specifically, 5.4% of cells (40.3% of reward-stable cells) were located before the
440 reward in UU, versus 7.3% of cells (26% of reward-stable cells) in UI (Figure 4c:ii; comparison UU/UI
441 proportions z-test $p = 3.4 \times 10^{-1}$, non significant). In the vicinity of the reward, we found 7% of cells
442 (51.1% of reward-stable cells) in UU, and 18.3% of cells (65.2% of reward-stable cells) in UI (Figure
443 4c:iii; comparison UU/UI proportions z-test $p = 3.4 \times 10^{-6}$, comparison UU<UI 1-sided proportion z-
444 test $p = 2.7 \times 10^{-6}$). Post-reward, similar percentages of reward-stable cells were found, with 4.8% of
445 cells (35.5% of reward-stable cells) in UU, and 5.3% of cells (18.8% of reward-stable cells) in UI (Figure
446 4c:iv; comparison UU/UI proportions z-test $p = 7.9 \times 10^{-1}$, non significant).

447 Given the over-representation of reward locations in both LU and EU, and our discovery that expected
448 uncertainty leads to an enhanced flexibility of this population, we sought to understand where the
449 previously reward-peaking cells moved to after the unexpected switch in UU and UI. For this, we explored
450 the post-switch peak locations of cells that peaked in the vicinity of the reward pre-switch. These differed
451 significantly between UU and UI (Figure 4e; distribution comparison using a Kolmogorov-Smirnov test
452 p-value $< 2.2 \times 10^{-308}$). The bimodal distribution for UU indicates a peak at the previous reward location;
453 by contrast, more reward-cells moved to the new reward location in UI. Quantifying whether the previous
454 reward location in UU is indeed over-represented, we found 0.9% of previously reward-peaking cells per
455 cm at the current reward location after the switch (comparison current>elsewhere 1-sided proportion z-
456 test $p < 2.2 \times 10^{-308}$) and 0.88% of those cells per cm peaking at the previous reward location (comparison
457 previous;elsewhere 1-sided proportion z-test $< 2.2 \times 10^{-308}$), while only 0.14% of previously reward
458 stable cells remapped elsewhere in the track after the switch (See figure 4f), confirming persistence of
459 the previous reward location in UU.

460 Building on the observation of an enhanced post-reward warped metric after UI compared to UU, we
461 turned to look into whether there was a difference between UU and UI in how the warped stability is
462 organized with respect to the reward. Investigation of the stability with respect to the warped reference
463 frame confirmed our earlier results, showing overall lower warped-stability in UU, with 26.2% of cells,
464 compared to UI, with 41% of cells (Figure 4d:i; comparison UU/UI proportions z-test $p = 6.51 \times$
465 10^{-5} , comparison UU<UI 1-sided proportion z-test $p = 3.26 \times 10^{-5}$). Similarly consistent with our
466 earlier results, no difference in warped-stability was found before the reward, with 10.1% (38.7% of all
467 warped-stable cells) in UU and 10.2% (24.8% of warped-stable) in UI (Figure 4d:ii; comparison UU/UI
468 proportions z-test $p = 9.8 \times 10^{-1}$, non-significant). In the vicinity of the reward, fewer cells were warped-
469 aligned in UU (7.4% of cells, 28.6% of warped-stable cells), compared to UI (17.9% of cells, 43.6% of
470 warped-stable cells) (Figure 4d:iii; comparison UU/UI proportions z-test $p = 2.9 \times 10^{-5}$, comparison
471 UU<UI 1-sided proportion z-test $p = 1.4 \times 10^{-5}$). Post-reward warped-stability was slightly different,
472 with only 8.6% of cells (32.8% of warped-stable cells) in UU, and 13% (31.7% of warped-stable cells) in
473 UI (Figure 4d:iv; comparison UU<UI 1-sided proportion z-test $p = 6.02 \times 10^{-2}$).

474 Overall, these results establish that starting from a state of high versus low expected uncertainty increased
475 the proportion of reward and warped place cells that moved to follow the reward after the unexpected
476 change in reward location. Starting from a state of low uncertainty, by contrast, led to a less flexible
477 representation in which reward location encoding place cells tended to remain at the location of the
478 initial reward, even after the unexpected change in reward location.

Fig. 4: Unexpected uncertainty in reward location highlights persistence of the previous reward location, EU features generalisation of reward encoding



479 a) Distribution of the locations of the peak activity of position-stable cells. The x-axis shows position
 480 along the track in cm. Bars show the percentage of position-stable cells having their peak activity in
 481 a position reference frame in the respective position-bin for UI (red) and UU (turquoise). Right insets
 482 show repeat of 3e) illustrating the cells counted in the histogram plot. Distribution comparison using a

483 Kolmogorov-Smirnov test $p = 0.47$, non significant.
484 b) Percentages of cells with stable peaks in a position reference frame: i: across the whole track (with a
485 maximum displacement of $\pm 15\text{cm}$; similar to 3h) comparison UU/UI proportions z-test $p = 5.14 \times 10^{-1}$,
486 non significant; ii: before the reward zone ($<-15\text{cm}$) before and after the switch (horizontal bar zone
487 in the insert); comparison UU/UI proportions z-test $p = 8.64 \times 10^{-2}$, comparison UU>UI 1-sided
488 proportion z-test $p = 4.32 \times 10^{-2}$; iii: in the vicinity of the reward zone ($-15\text{cm}/+20\text{cm}$) before and
489 after the switch (tilted bar zone in the insert); comparison UU/UI proportions z-test $p = 2.27 \times 10^{-1}$,
490 non significant; iv) after the reward zone ($>+20\text{cm}$) both before and after the switch (vertical bar zone
491 in the insert); comparison UU/UI proportions z-test $p = 9.52 \times 10^{-1}$, non significant.
492 c) Percentages of cells with stable peaks in a reward reference frame: i: across the whole track; com-
493 parison UU/UI proportions z-test $p = 1.26 \times 10^{-6}$, comparison UU<UI 1-sided proportion z-test
494 $p = 8.65 \times 10^{-7}$; ii: before the reward zone ($<-15\text{cm}$) before and after the switch; comparison UU/UI
495 proportions z-test $p = 4.04 \times 10^{-1}$, non significant; iii: in the vicinity of the reward ($-15\text{cm}/+20\text{cm}$)
496 before and after the switch; comparison UU/UI proportions z-test $p = 1.73 \times 10^{-6}$, comparison UU<UI
497 1-sided proportion z-test $p = 8.65 \times 10^{-7}$; iv) after the reward ($>+20\text{cm}$) before and after the switch;
498 comparison UU/UI proportions z-test $p = 4.14 \times 10^{-1}$, non significant.
499 d) Percentages of cells with stable peaks in a warped reference frame: i: across the whole track; UU/UI
500 proportions z-test $p = 6.51 \times 10^{-5}$, comparison UU<UI 1-sided proportion z-test $p = 3.26 \times 10^{-5}$; ii:
501 before the reward (<-2 warped units) before and after the switch; comparison UU/UI proportions z-test
502 $p = 8.35 \times 10^{-1}$, non-significant; iii: in the vicinity of the reward ($-2/+3$ warped units) before and after
503 the switch, comparison UU/UI proportions z-test $p = 2.9 \times 10^{-5}$, comparison UU<UI 1-sided proportion
504 z-test $p = 1.4 \times 10^{-5}$; iv: after the reward ($>+3$ warped units) before and after the switch; comparison
505 UU/UI proportions z-test $p = 1.2 \times 10^{-1}$, comparison UU<UI 1-sided proportion z-test $p = 6.2 \times 10^{-2}$.
506 e) Distribution of the peak location relative to post-switch reward of the cells that peaked in the vicinity
507 of ($-15, +20\text{cm}$) the reward before the switch for UI (red) and UU (turquoise). The x-axis shows
508 bins of position along the track relative to post-switch reward. Cells peaking at 0cm follow the reward
509 through the switch. Right insets repeat figure 3e), illustrating the cells counted in the histogram plot
510 with vertical bars. Distribution comparison using a Kolmogorov-Smirnov test p-value $< 2.2 \times 10^{-308}$.
511 f) Percentages per cm of previously reward peaking cells after the switch, that stay reward
512 peaking (current, rightward tilt), that stay peaking at the previous reward (previous, leftward
513 tilt), or that move elsewhere (else, plain bar) for UU. Comparison current>else 1-sided propor-
514 tions z-test $< 2.2 \times 10^{-308}$, comparison previous>else 1-sided proportions z-test $< 2.2 \times 10^{-308}$.

515

516

517 Discussion

518 We imaged dorsal CA1 while mice navigated in a virtual reality corridor in which reward became avail-
519 able according to one of a number of distributions of spatial location. These induced different forms
520 of uncertainty that we studied across three positional reference frames: environment-centered, reward-
521 centered, and a combined metric where the reward and the end of the track anchored experience, with
522 the hippocampus generating what amounts to a warped spatial metric. We found that reward-dedicated
523 place cells adapted flexibly to trial-by-trial changes in reward location, with this adaptability extending
524 to larger, unexpected reward shifts, especially in reward-based and warped reference frames. This was
525 not observed in animals conditioned to low uncertainty. Initial stability in reward location did not lead
526 to more global remapping in a position reference frame when the reward subsequently moved, but led to
527 persistence of previous reward location. These results contribute to our understanding of the structure
528 of cognitive maps.
529 Our results expand on previous findings about reward-dedicated place cells(Dupret et al, 2010; Gau-
530 thier and Tank, 2018; Hollup et al, 2001; Jarzebowski et al, 2022; Sosa and Giocomo, 2021), showing
531 their ability to adapt to single-trial changes in reward location. This is consistent with previous electro-
532 physiological results highlighting abstract goal populations in the hippocampus (McKenzie et al, 2013;
533 McNaughton and Bannerman, 2024; Zeithamova et al, 2018), and behavioral results showing that the

534 hippocampus is required for single-shot learning of new goal locations (Bast et al, 2009; Kleinknecht
535 et al, 2012; Morris et al, 1990; Sosa and Giocomo, 2021; Steele and Morris, 1999; Tessereau et al, 2021).
536 Such cells have been suggested in models (Burgess and O'Keefe, 1996; Foster et al, 2000; Tessereau et al,
537 2021) as serving flexible behavioural adaptation, for example acting as a reference point for vector-based
538 navigation (Burgess et al, 1995; Foster et al, 2000; Tessereau et al, 2021), or uncertainty resolution, to
539 guide prediction (Burgess et al, 1995). Our results converge with a recent paper investigating the effect
540 of multiple similar changes in reward location on the reward population codes of the hippocampus. By
541 changing the reward location between multiple phase of stable reward locations, (Sosa et al, 2023) found
542 that place cells can organise within reward-centered sequences which recruit more cells as the reward loca-
543 tion changes day-by-day. Although the authors focus on reward population codes, we can now interpret
544 their results in terms of expected uncertainty, induced by block-by-block changes in reward. The extra
545 recruitment of reward cells would then be an instance of the excess of reward-following cells apparent in
546 our UI condition. Similar findings suggest that reward-induced behavioral changes create a landmark-
547 based reference frame in the hippocampus (Vaidya et al, 2023), with over-representation of salient cues
548 extending beyond rewards (Tanni et al, 2022; Vaidya et al, 2023). This over-representation likely arises
549 from distinct mechanisms for landmarks and rewards (Sato et al, 2020).

550 In conditions of EU, we observed a warped spatial metric consistent with past studies(Gothard et al,
551 1996), where the track segment following the reward and preceding the teleportation zone was renor-
552 malized. Whether the warped metric is the reflection of stereotypical behavioural sequences induced by
553 having to stop to consume the reward, and running until the end of the track, or whether the reward
554 itself is a sufficient anchor to induce such a warped metric, remains unclear. Comparable place map
555 warping has been seen when mice were exposed to gradually changing visual patterns Plitt and Gio-
556 como (2021) or visual boundaries (Leutgeb et al, 2005a), creating continuous place cell activity profiles.
557 In contrast, abrupt remapping occurred when mice were only familiar with extreme conditions, parallel-
558 ing the response to unexpected uncertainty in the reward reference frame in our study. The integration
559 of homogeneous episodes within continuous, possibly warped, metrics is also consistent with suggested
560 roles of the hippocampus as a comparator (Kumaran and Maguire, 2007; Vinogradova, 2001) – perhaps
561 responding to the conflict between external cues and internal, self-motion cues (Gothard et al, 1996),
562 or intrinsic reward encoding. Indeed, warped metrics provide an efficient way to associate discontiguous
563 events (Wallenstein et al, 1998), and may promote one-shot decision making by enhancing state-space
564 separability (McKenzie et al, 2014; Muzzio et al, 2009; Nitz, 2009; Sun et al, 2023).

565 Our finding that unexpected uncertainty did not induce greater position remapping than expected uncer-
566 tainty contradicts our initial hypothesis, which anticipated more extensive remapping under surprise.
567 By contrast, previous work has suggested that greater surprise is associated with greater remapping
568 (Sanders et al, 2020), and indeed drastic changes in context, such as the visual environment (Anderson
569 and Jeffery, 2003; Bostock et al, 1991; Kentros et al, 1998; Leutgeb et al, 2005b; Muller and Kubie, 1987;
570 Sanders et al, 2020; Sheffield and Dombeck, 2019) can lead to substantial degrees of remapping. It may be
571 that surprising reward locations and sensory mispredictions (Sanders et al, 2020) are treated somewhat
572 independently. This would be consistent with the greater degree of reward-related and warped-metric
573 remapping in UU compared to UI, suggesting that remapping can occur independently in different ref-
574 erence frames, and building on existing results shedding light on overlapping reference frames in spatial
575 navigation tasks (Zinyuk et al, 2000).

576 In UU, we found that the population of place cells previously peaking at the reward became bimodally
577 distributed around the previous and new reward location. This suggests that repeated experience of a
578 specific episode could lead to cells becoming specific to single episodes, akin to splitter cells (Wood et al,
579 2000), but in reward reference-frames, similar to the finding in (McKenzie et al, 2013). In contrast, in
580 UI, reward-aligned cells and warped-aligned cells moved flexibly to the new goal location. This confirms
581 a previous result suggesting independence of reward and position reference frames in rats (Aoki et al,
582 2019). We might interpret this difference in terms of generalization: context-specific representations are
583 probably well suited for efficient decision making when environments distinctly differ, as in the transition
584 in UU. However, under EU, the multiple reward locations are tied under a common, moderately compact,
585 distribution. Rather than exhausting capacity by representing each separately, the hippocampal solution

586 appears to be to have similar events share representations, by adopting metrics that encapsulate shared
587 aspects of experience. This then generalizes when the reward location shifts yet further in UI.

588 We focused our analyses on peak place cell activity, but future work could explore subtleties in firing
589 rates (Sanders et al, 2019), and the relationship with theta rhythms (Chadwick et al, 2015). We only
590 considered stable place cells before and after transitions; examining population turnover could yield
591 further insights. To ensure robustness, we emphasized average spatial receptive fields, but tracking fast
592 reward location changes remains essential. Finally, repeated switches, like those in UU, may eventually
593 become expected, highlighting the need to understand how unknown unknowns transition to known
594 unknowns in stochastic environments.

595 Future work should focus on deciphering the implementation processes underlying our findings. Plateau
596 potentials generated by synchronized inputs from the entorhinal cortex and CA3 can lead to the formation
597 of new feature-selective cells (Bittner et al, 2015). Furthermore, recent studies have highlighted enhanced
598 reward-reference frame coding in the lateral entorhinal cortex (LEC) (Issa et al, 2024), and medial
599 entorhinal cells are also attracted to goals (Boccaro et al, 2019). Given that grid cells provide different
600 spatial metrics and can anchor to task-relevant features (Peng et al, 2023), it would be natural to explore
601 grid cell activity in the various conditions of our study. This might shed light on the structured diversity
602 of CA1 place cells selectivity.

603 Task-relevant place cells selectivity could be driven by neuromodulatory inputs (Kaufman et al, 2020;
604 Palacios-Filardo and Mellor, 2019; Palacios-Filardo et al, 2021). Evidence shows that acetylcholine,
605 dopamine, noradrenaline and serotonin neuromodulatory systems provide signals associated with expec-
606 tation, error and uncertainty, with their release reconfiguring hippocampal (and wider cortical) neuronal
607 circuits to enable the update of estimates and memories (Dayan, 2012). Under this framework, the release
608 of specific combinations of neuromodulators potentially codes for different types of uncertainty and could
609 thereby influence the degree and type of place cell reorganisation. Indeed, dopaminergic and noradren-
610 ergic projections to CA1 from ventral tegmental area and locus coeruleus convey information about
611 reward prediction errors (Cohen et al, 2012; Fiorillo et al, 2003; Schultz et al, 1997) and surprise (Fiorillo
612 et al, 2003; Heer and Mark, 2023; Kaufman et al, 2020; McNamara et al, 2014) and can causally shape
613 reward-related CA1 reorganisation (Kaufman et al, 2020; Krishnan et al, 2022), specifically in response
614 to high reward prediction errors (Michon et al, 2021). Synaptic plasticity is the mechanism for place
615 cell reorganisation and is regulated by neuromodulators in multiple ways (Palacios-Filardo and Mellor,
616 2019). For example, acetylcholine reprioritises entorhinal and CA3 inputs to CA1 reducing the inter-
617 internal representations from CA3 and enhancing external sensory input from entorhinal cortex (Hasselmo,
618 2006; Hasselmo and McGaughy, 2004; Palacios-Filardo et al, 2021) whilst also reconfiguring inhibitory
619 networks (Haam et al, 2018; Leão et al, 2012) and enhancing dendritic excitability and synaptic plastic-
620 ity (Buchanan et al, 2010; Dennis et al, 2016; Gu and Yakel, 2011; Teles-Grilo Ruivo and Mellor, 2013;
621 Williams and Fletcher, 2019) in response to surprising events (Mineur et al, 2022; Ruivo et al, 2017).
622 Thus, neuromodulators are an attractive mechanism linking detection of uncertainty to the update of
623 hippocampal representations with new information.

624 In conclusion, we exploited the relative transparency of the spatial activity of hippocampal place cells in
625 order to examine the effects of different forms of uncertainty about the location of reward, and, equally,
626 used these different forms of uncertainty to enrich our understanding of the hippocampal code for space.
627 Place cells exhibited impressive adaptation to the diverse statistical contingencies, with sub-populations
628 adopting what we can see as different relevant reference frames. This sharpens the hippocampus's role
629 as not only a spatial navigator but also a flexible processor of uncertainty. By offering multiple reference
630 frames depending on task-relevant features like reward, the hippocampus provides a robust framework
631 for adapting to both expected and unexpected uncertainty. This flexibility suggests a novel mechanism
632 by which the brain supports rapid decision-making under uncertainty — crucial for survival in changing
633 environments — and provides downstream circuits with a computationally sophisticated representation
634 which can afford an attractive combination of specialization and generalization.

635 Methods

636 Mouse surgery

637 All experiments were approved and conducted in accordance with the Northwestern University Animal
638 Care and Use Committee. Seven male P56-P63 mice (C57BL/6J, Jackson Laboratory, stock no.000664)
639 were used in the experiments. To induce the expression of a calcium indicator, mice were first injected
640 with AAV virus expressing jGCaMP8m (AAV1-syn-FLEX-jGCaMP8m-WPRE) ([Zhang et al, 2023](#)) into
641 dorsal CA1 region of the right hippocampus (1.8mm lateral, 2.3mm caudal of Bregma, 1.25mm below the
642 dura surface). After the injection, mice first recovered with ad libitum water for 1-2 days and then were
643 subject to water restriction (0.8-1.2ml per day) until the end of all experiments. The weight of all mice
644 was monitored and kept between 75%-80% of the original weight. After 3-5 days under water restriction,
645 hippocampal cannula implant surgeries were performed above the injection site to allow optical access to
646 dorsal CA1 of the hippocampus, as previously described ([Dombeck et al, 2010](#)). Briefly, cortex above the
647 dorsal hippocampus was aspirated until the white matter of the external capsule was exposed. Phosphate
648 buffer solution (PBS) was repeatedly applied until the bleeding stopped and a small drop of Kwik-Sil
649 was applied to the tissue surface before the cannula was inserted. A head-plate and a ring were cemented
650 on the skull using Meta-bond. Proper analgesic and anesthetic procedures were carried out according to
651 the animal protocol. All mice were allowed to recover for 5-7 days before the start of behavioral training.

652 Virtual reality and behavior task

653 Seven male mice were first separated into two groups, three and four mice for each group respectively.
654 All mice were first habituated in the head-fixed VR setup ([Sheffield et al, 2017](#)) (with screen off) for one
655 session (45 minutes), during which a couple of water rewards were delivered to the mice randomly to
656 familiarize them with the lick port. Beginning from the second session, VR screens were turned on and
657 both groups of mice were first trained in one visual environment to perform the URTask. Each training
658 session lasted 45min to 1hr depending on how many laps the mice had run. Mice were considered well-
659 trained if they satisfied both criteria: 1. They had to run at least 1 2 laps per minute; 2. They had to
660 have anticipatory licking before the reward (anticipatory licking) for at least 50% of the laps; 3. Their
661 behaviour is stable for three consecutive sessions, as measured by the average correlation coefficient of
662 velocity and licking patterns across all laps. All mice reached this performance level after 8-10 session of
663 training.

664 Two-photon imaging

665 Two-photon calcium imaging of dorsal CA1 neurons was performed using a custom-built moveable objec-
666 tive microscope, with a 40x /0.8NA water immersion objective (LUMPlanFL N 3 40/0.8 W, Olympus),
667 as described previously ([Dombeck et al, 2010](#); [Sheffield et al, 2017](#)). The control software for two-photon
668 scanning was ScanImage 5.1(Vidrio Technologies). Average laser power after the objective was around
669 60 100mW. Time-series movies of 12000 24000 frames, 512 x 256 pixels were acquired at 30Hz frame-
670 rate. A Digidata1440A (Molecular Device) data acquisition system (Clampex 10.3) was used to record
671 (at 1 kHz) and synchronize behavioral variables (licking, linear track position, velocity and reward deliv-
672 ery) with two-photon imaging frame time. During the same session, the imaging field stayed the same.
673 During the consecutive imaging sessions, the imaging fields were not identical, although there might be
674 overlap between the imaging fields.

675 Image processing and ROI selection

676 Two-photon imaging time-series movies were first imported into Suite2p ([Pachitariu et al, 2017](#)) for rigid
 677 and non-rigid motion-correction. Putative cell (region of interest, ROIs) were extracted from motion-
 678 corrected movies using Suite2p.

Table 1: Suite2P Parameters

Parameter	Value	Parameter	Value	Parameter	Value
nplanes	1	nchannels	1	functional_chan	1
tau	0.6	fs	30	do_bidiphase	0
bidiphase	0	multiplane_parallel	0	ignore_flyback	-1
preclassify	0	save_mat	1	save_NWB	0
combined	1	reg_rig	1	reg_tif_chan2	0
aspect	1	delete_bin	0	move_bin	0
do_registration	1	align_by_chan	1	nimg_init	300
batch_size	500	smooth_sigma	1.15	smooth_sigma_time	0
maxregshift	0.1	th_badframes	1	keep_movie_raw	0
two_step_registration	0	nonrigid	1	block_size	32,64
snr_thresh	1.2	maxregshiftNR	5.0	1Preg	0
spatial_hp_reg	32	pre_smooth	0	spatial_taper	40.0
roidetect	1	denoise	1	spatial_scale	0
threshold_scaling	2.0	max_overlap	0.75	max_iterations	20
high_pass	100.0	spatial_hp_detect	25	anatomical_only	0.0
diameter	0				

679 Extracted ROI fluorescence traces were then exported from suite2P and imported into MATLAB for
 680 extracting significant calcium transients ([Dombeck et al, 2010](#)). For each ROI, the potential signal con-
 681 tamination from the surrounding neuropil was subtracted (after multiplied by a factor of 0.7) from the
 682 raw fluorescence signal. Slow time-course changes in the neuropil-corrected traces were removed by cal-
 683 culating the distribution of fluorescence in a 20-s time window around each time point and subtracting
 684 the 8th percentile value of the distribution. The baseline subtracted traces were then subjected to the
 685 analysis of the ratio of positive- to negative-going transients of various amplitudes and durations. This
 686 resulted in the identification of significant transients with less than 1% false positive rate. The signifi-
 687 cant transients were left untouched while all other values in the trace were set to 0. The resulting traces
 688 (referred to as 'changes in fluorescence' in the following section) of all ROIs were used for further data
 689 analysis.

690 Place cell spatial information test and identification

691 Fluorescence tuning maps were created by binning the position across the track into 60 bins and identi-
 692 fying the mean change in fluorescence when the animal was moving at least 0.1 cm per second. To test
 693 whether a cell is a place cell, we computed the spatial information (I) in bits per action potential for the
 694 fluorescence tuning map ([Climer and Dombeck, 2021](#)):

$$I = \frac{1}{\bar{f}} \sum_{i=1}^N f_i \cdot PX(x_i) \log_2 \left(\frac{f_i}{\bar{f}} \right)$$

695 where \bar{f} is the mean change in fluorescence, N is the number of bins, f_i is the fluorescence change in
 696 the i^{th} spatial bin, and $PX(x_i)$ is the probability that the animal is in the i^{th} spatial bin. To build a
 697 null distribution of information, we circularly shuffled the fluorescence trace with a minimum shift of 15
 698 seconds and recalculated the tuning map 1000 times. A cell was considered a significant place cell if it
 699 had higher information than 99% of these shuffled epochs, had an information value of at least 0.5 bits
 700 per action potential.

701 Trial inclusion criteria

702 The position of reward consumption was defined as the first lick after reward delivery on every trial. As
703 animals were engaged in the task, on most trials, licking was very close to reward delivery. The reward
704 zone was then defined as the zone between the most proximal reward consumption position, until the
705 most distal reward consumption position.

706 In order to obtain a meaningful reward zone, we excluded 2.5% of the trials (35 out of 1376 total trials
707 included in this paper) that were outlier in the distance at which the reward was consumed after delivery.
708 This selection criteria generated a threshold of approximately 11 cm between reward delivery and reward
709 consumption, therefore excluding trials in which the reward was not consumed, or was consumed after this
710 distance. Supplementary Figure ?? shows the histogram of consumption distance from reward delivery,
711 which we also consider as a marker for engagement in the task.

712 Trial separation

713 We separated proximal, middle and distal rewards by dividing the reward zone in 3 bins of identical
714 length. The trials in which the reward was consumed in the first (resp. second, third) bin were labelled
715 'proximal' (resp. 'middle', 'distal').

716 Behaviour analysis

717 We excluded from all analyses the teleportation phase (during which the screen went black), and all
718 datapoint at which the velocity fell under 0.1 cm/s.

719 Analyses were performed using custom Python code. To calculate the lick rate and velocity patterns
720 (figures 2a;b, figure 3a;b), we averaged the lick rate and velocity trace, downsampled at 30 Hz, over a
721 position vector covering all position values (from 0 to 3m) with a bin size of 10 cm. To compute averages,
722 we extracted the values of the behavioral variables for the cases in which the position trace was within
723 each position bin, and computed averages weighted by the time spent in each position bin. For figure
724 2a, for every session average-value, we computed the average over all trials for LU and divided it by the
725 maximum value over the session. We then averaged this value across sessions and animals. For figure
726 2b, for EU, we computed the average on proximal, middle and distal trials, and normalised it to the
727 maximum value of the average computed over the full session. We then averaged these values across
728 sessions and animals.

729 Place cell activity analysis

730 For all place cells analyses, we excluded periods in which the animal ran with a velocity less than 1cm/s,
731 and the teleportation corridor. For figure 2d;e, Figure 3c;d, and Figure 3b, each place cell's activity was
732 averaged similarly to behavioural variables: the average place cell activity over the session was computed
733 by averaging the activity per position bin across every trial weighted by the time spent in each position
734 bin. Place maps in figures 2d;e show the average activity of cells on odd trials, ordered based on the
735 location of the peak activity on even trials. Place map plots were produced by normalizing the average
736 activity of every cell on odd trials by its maximum value.

737 For switch sessions (place maps in figures 3c;d), place map plots before the switch were produced by
738 normalising the average activity of every cell on all trials before the switch by its maximum value.
739 Similarly, place map plots after the switch were produced by normalising the average activity of every
740 cell on all trials after the switch by its maximum value.

741 Peak activity analysis

- 742 The position of maximum activity was extracted as the location of the 10cm bin in which the average
743 activity of the cell was greatest. For figure 2e, we considered the average activity on proximal and distal
744 groups of trials. For figure 3e, the average was computed over trials before (x-axis) and after (y-axis) the
745 reward switch separately.
- 746 For figures 2f and 3e, the x and y coordinates are fitted with gaussian_kde function from the scipy.stats
747 module, which estimates the probability density function (PDF) of a random variable in a non-parametric
748 way. The heatmap shows this Gaussian fitted density estimation.

749 Reward and warped reference frame

- 750 The reward reference frame was obtained by computing positions relative to the position of the
751 consumption of the reward at every trial, and using 10cm position bins.
- 752 The warped reference frame was obtained by creating a warped vector interpolating the position in 20
753 bins between the start of the track and the reward location, and 20 bins from the reward location to the
754 end of the track at every trial. These new bins were then the basis for all averages.

755 Place cell identification

- 756 In figure 2g, 'Position-stable' cells were place cells that passed the place cell test and which position of
757 peak of activity on proximal and distal trials were at most 15cm apart.
- 758 In figure 3f, 'Position-stable' cells were place cells that passed the place cell test before and after the
759 switch and which position of peak of activity before and after the switch were at most 15cm apart.
- 760 In figure 3g, 'reward-peaking' cells were place cells that passed the place cell test before and after the
761 switch and whose positions of peak of activity in the reward reference frame before and after the switch
762 were between -15 and +20 cm.
- 763 In figure 3h, 'Warped' place cells were place cells that passed the place cell test before and after the
764 switch and which position of peak of activity in the warped reference frame before and after the switch
765 were identical with + or - 3 warped units, and which position of maximum activity followed the reward.

766 Cell percentage and cell percentage per cm

767 Statistical analyses

- 768 All statistics were done using the package 'statsmodels' in python.
- 769 To compare percentages, we used the percentage z-test, and for 1-sided proportion z-test to test for
770 directionality. To compare distributions, we used the Kolmogorov-Smirnov test.

771 Data availability

- 772 The data will be made freely available following publication.

773 Code availability

774 All computer programs will be made freely available following publication.

775 Supplementary material

776 Please see supplementary figures.

777 Acknowledgements

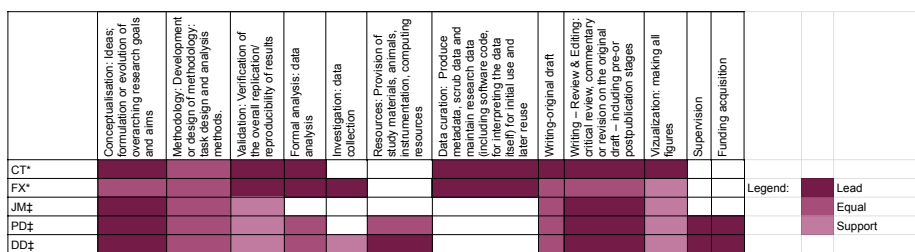
778 We are grateful to Claudia Clopath, Matt Jones, Zach Mainen, Tony Pickering and Mark Walton for
779 influential discussions about the design of the task. We thank Marielena Sosa, Mark Plitt and Lisa
780 Giocomo for sharing their results prior to publication.

781 Funding

782 Funding was from the Max Planck Society (CT, PD) and the Humboldt Foundation (PD). PD is a
783 member of the Machine Learning Cluster of Excellence, EXC number 2064/1 – Project number 39072764
784 and of the Else Kröner Medical Scientist Kolleg “ClinbrAIn: Artificial Intelligence for Clinical Brain
785 Research”. Funding for JRM from Wellcome Trust (101029/Z/13/Z) and Biotechnology and Biological
786 Sciences Research Council (BBSRC, BB/V001728/1, BB/N013956/1). FX was supported by National
787 Institute of Mental Health Training Program in Neurobiology of Information Storage (T32MH067564)
788 predoctoral fellowship.

789 Author Credit Contribution

Fig. 5: CRediT



CRediT contribution matrix. Color code refers to the level of contribution per category, as previously used (Tay, 2021). Categories reflect the ones published in the original CRediT taxonomy in (Brand et al, 2015).

790 Conflict of interest/Competing interests

791 The authors declare no conflict of interest.

792 References

- 793 Anderson MI, Jeffery KJ (2003) Heterogeneous modulation of place cell firing by changes in context.
794 Journal of Neuroscience 23(26):8827–8835
- 795 Aoki Y, Igata H, Ikegaya Y, et al (2019) The integration of goal-directed signals onto spatial maps of
796 hippocampal place cells. Cell reports 27(5):1516–1527
- 797 Bast T, Wilson IA, Witter MP, et al (2009) From rapid place learning to behavioral performance: a key
798 role for the intermediate hippocampus. PLoS biology 7(4):e1000089
- 799 Behrens TE, Woolrich MW, Walton ME, et al (2007) Learning the value of information in an uncertain
800 world. Nature neuroscience 10(9):1214–1221
- 801 Best PJ, White AM, Minai A (2001) Spatial processing in the brain: the activity of hippocampal place
802 cells. Annual review of neuroscience 24(1):459–486
- 803 Bittner KC, Grienberger C, Vaidya SP, et al (2015) Conjunctive input processing drives feature selectivity
804 in hippocampal ca1 neurons. Nature neuroscience 18(8):1133–1142
- 805 Boccara CN, Nardin M, Stella F, et al (2019) The entorhinal cognitive map is attracted to goals. Science
806 363(6434):1443–1447
- 807 Bostock E, Muller RU, Kubie JL (1991) Experience-dependent modifications of hippocampal place cell
808 firing. Hippocampus 1(2):193–205
- 809 Brand A, Allen L, Altman M, et al (2015) Beyond authorship: Attribution, contribution, collaboration,
810 and credit. Learned Publishing 28(2)
- 811 Buchanan KA, Petrovic MM, Chamberlain SE, et al (2010) Facilitation of long-term potentiation by
812 muscarinic m1 receptors is mediated by inhibition of sk channels. Neuron 68(5):948–963
- 813 Burgess N, O'Keefe J (1996) Neuronal computations underlying the firing of place cells and their role in
814 navigation. Hippocampus 6(6):749–762
- 815 Burgess N, Recce M, O'Keefe J (1995) Hippocampus: spatial models. The handbook of brain theory and
816 neural networks pp 468–472
- 817 Chadwick A, van Rossum MC, Nolan MF (2015) Independent theta phase coding accounts for ca1
818 population sequences and enables flexible remapping. Elife 4:e03542
- 819 Climer JR, Dombeck DA (2021) Information Theoretic Approaches to Deciphering the Neural Code with
820 Functional Fluorescence Imaging. eNeuro 8(5)
- 821 Cohen JY, Haesler S, Vong L, et al (2012) Neuron-type-specific signals for reward and punishment in
822 the ventral tegmental area. nature 482(7383):85–88
- 823 Cohen JY, Amoroso MW, Uchida N (2015) Serotonergic neurons signal reward and punishment on
824 multiple timescales. Elife 4:e06346
- 825 Dayan P (2012) Twenty-five lessons from computational neuromodulation. Neuron 76(1):240–256

- 826 Dennis SH, Pasqui F, Colvin EM, et al (2016) Activation of muscarinic m₁ acetylcholine receptors induces
827 long-term potentiation in the hippocampus. *Cerebral cortex* 26(1):414–426
- 828 Dombeck DA, Harvey CD, Tian L, et al (2010) Functional imaging of hippocampal place cells at cellular
829 resolution during virtual navigation. *Nature neuroscience* 13(11):1433–1440
- 830 Dupret D, O'Neill J, Pleydell-Bouverie B, et al (2010) The reorganization and reactivation of hippocampal
831 maps predict spatial memory performance. *Nature neuroscience* 13(8):995–1002
- 832 Fiorillo CD, Tobler PN, Schultz W (2003) Discrete coding of reward probability and uncertainty by
833 dopamine neurons. *Science* 299(5614):1898–1902
- 834 Foster DJ, Morris RG, Dayan P (2000) A model of hippocampally dependent navigation, using the
835 temporal difference learning rule. *Hippocampus* 10(1):1–16
- 836 Frank LM, Stanley GB, Brown EN (2004) Hippocampal plasticity across multiple days of exposure to
837 novel environments. *Journal of Neuroscience* 24(35):7681–7689
- 838 Gauthier JL, Tank DW (2018) A dedicated population for reward coding in the hippocampus. *Neuron*
839 99(1):179–193
- 840 Gothard KM, Skaggs WE, McNaughton BL (1996) Dynamics of mismatch correction in the hippocampal
841 ensemble code for space: interaction between path integration and environmental cues. *Journal of*
842 *Neuroscience* 16(24):8027–8040
- 843 Gu Z, Yakel JL (2011) Timing-dependent septal cholinergic induction of dynamic hippocampal synaptic
844 plasticity. *Neuron* 71(1):155–165
- 845 Haam J, Zhou J, Cui G, et al (2018) Septal cholinergic neurons gate hippocampal output to entorhinal
846 cortex via oriens lacunosum moleculare interneurons. *Proceedings of the National Academy of Sciences*
847 115(8):E1886–E1895
- 848 Hasselmo ME (2006) The role of acetylcholine in learning and memory. *Current opinion in neurobiology*
849 16(6):710–715
- 850 Hasselmo ME, McGaughy J (2004) High acetylcholine levels set circuit dynamics for attention and
851 encoding and low acetylcholine levels set dynamics for consolidation. *Progress in brain research*
852 145:207–231
- 853 Heer CM, Mark E (2023) Distinct catecholaminergic pathways projecting to hippocampal ca1 transmit
854 contrasting signals during behavior and learning. *bioRxiv*
- 855 Hill A (1978) First occurrence of hippocampal spatial firing in a new environment. *Experimental*
856 *neurology* 62(2):282–297
- 857 Hollup SA, Molden S, Donnett JG, et al (2001) Accumulation of hippocampal place fields at the goal
858 location in an annular watermaze task. *Journal of Neuroscience* 21(5):1635–1644
- 859 Hsu M, Bhatt M, Adolphs R, et al (2005) Neural systems responding to degrees of uncertainty in human
860 decision-making. *Science* 310(5754):1680–1683
- 861 Hüllermeier E, Waegeman W (2021) Aleatoric and epistemic uncertainty in machine learning: An
862 introduction to concepts and methods. *Machine learning* 110(3):457–506
- 863 Issa JB, Radvansky BA, Xuan F, et al (2024) Lateral entorhinal cortex subpopulations represent
864 experiential epochs surrounding reward. *Nature neuroscience* 27(3):536–546

- 865 Jarzebowski P, Hay YA, Grewe BF, et al (2022) Different encoding of reward location in dorsal and
866 intermediate hippocampus. *Current Biology* 32(4):834–841
- 867 Kaufman AM, Geiller T, Losonczy A (2020) A role for the locus coeruleus in hippocampal ca1 place cell
868 reorganization during spatial reward learning. *Neuron* 105(6):1018–1026
- 869 Kentros C, Hargreaves E, Hawkins RD, et al (1998) Abolition of long-term stability of new hippocampal
870 place cell maps by nmda receptor blockade. *Science* 280(5372):2121–2126
- 871 Kleinknecht KR, Bedenk BT, Kaltwasser SF, et al (2012) Hippocampus-dependent place learning enables
872 spatial flexibility in c57bl6/n mice. *Frontiers in behavioral neuroscience* 6:87
- 873 Krishnan S, Heer C, Cherian C, et al (2022) Reward expectation extinction restructures and degrades
874 ca1 spatial maps through loss of a dopaminergic reward proximity signal. *Nature communications*
875 13(1):6662
- 876 Kumaran D, Maguire EA (2007) Which computational mechanisms operate in the hippocampus during
877 novelty detection? *Hippocampus* 17(9):735–748
- 878 Leão RN, Mikulovic S, Leão KE, et al (2012) Olm interneurons differentially modulate ca3 and entorhinal
879 inputs to hippocampal ca1 neurons. *Nature neuroscience* 15(11):1524–1530
- 880 Leutgeb JK, Leutgeb S, Treves A, et al (2005a) Progressive transformation of hippocampal neuronal
881 representations in “morphed” environments. *Neuron* 48(2):345–358
- 882 Leutgeb S, Leutgeb JK, Barnes CA, et al (2005b) Independent codes for spatial and episodic memory in
883 hippocampal neuronal ensembles. *Science* 309(5734):619–623
- 884 Markus EJ, Qin YL, Leonard B, et al (1995) Interactions between location and task affect the spatial
885 and directional firing of hippocampal neurons. *Journal of Neuroscience* 15(11):7079–7094
- 886 McGuire JT, Nassar MR, Gold JI, et al (2014) Functionally dissociable influences on learning rate in a
887 dynamic environment. *Neuron* 84(4):870–881
- 888 McKenzie S, Robinson NT, Herrera L, et al (2013) Learning causes reorganization of neuronal fir-
889 ing patterns to represent related experiences within a hippocampal schema. *Journal of Neuroscience*
890 33(25):10243–10256
- 891 McKenzie S, Frank AJ, Kinsky NR, et al (2014) Hippocampal representation of related and opposing
892 memories develop within distinct, hierarchically organized neural schemas. *Neuron* 83(1):202–215
- 893 McNamara CG, Tejero-Cantero Á, Trouche S, et al (2014) Dopaminergic neurons promote hippocampal
894 reactivation and spatial memory persistence. *Nature neuroscience* 17(12):1658–1660
- 895 McNaughton N, Bannerman D (2024) The homogenous hippocampus: How hippocampal cells process
896 available and potential goals. *Progress in neurobiology* p 102653
- 897 Michon F, Krul E, Sun JJ, et al (2021) Single-trial dynamics of hippocampal spatial representations are
898 modulated by reward value. *Current Biology* 31(20):4423–4435
- 899 Mineur YS, Mose TN, Vanopdenbosch L, et al (2022) Hippocampal acetylcholine modulates stress-related
900 behaviors independent of specific cholinergic inputs. *Molecular psychiatry* 27(3):1829–1838
- 901 Morris RGM, Davis S, Butcher S (1990) Hippocampal synaptic plasticity and nmda receptors: a role in
902 information storage? *Philosophical Transactions of the Royal Society of London Series B: Biological*
903 *Sciences* 329(1253):187–204

- 904 Moser EI, Kropff E, Moser MB (2008) Place cells, grid cells, and the brain's spatial representation system.
905 Annu Rev Neurosci 31(1):69–89
- 906 Muller R (1996) A quarter of a century of place cells. Neuron 17(5):813–822
- 907 Muller RU, Kubie JL (1987) The effects of changes in the environment on the spatial firing of hippocampal
908 complex-spike cells. Journal of Neuroscience 7(7):1951–1968
- 909 Muzzio IA, Kentros C, Kandel E (2009) What is remembered? role of attention on the encoding and
910 retrieval of hippocampal representations. The Journal of physiology 587(12):2837–2854
- 911 Nassar MR, McGuire JT, Ritz H, et al (2019) Dissociable forms of uncertainty-driven representational
912 change across the human brain. Journal of Neuroscience 39(9):1688–1698
- 913 Nitz D (2009) Parietal cortex, navigation, and the construction of arbitrary reference frames for spatial
914 information. Neurobiology of learning and memory 91(2):179–185
- 915 O'Keefe J, Dostrovsky J (1971) The hippocampus as a spatial map: preliminary evidence from unit
916 activity in the freely-moving rat. Brain research
- 917 Pachitariu M, Stringer C, Dipoppa M, et al (2017) Suite2p: beyond 10,000 neurons with standard two-
918 photon microscopy. bioRxiv
- 919 Palacios-Filardo J, Mellor JR (2019) Neuromodulation of hippocampal long-term synaptic plasticity.
920 Current opinion in neurobiology 54:37–43
- 921 Palacios-Filardo J, Udkakis M, Brown GA, et al (2021) Acetylcholine prioritises direct synaptic inputs
922 from entorhinal cortex to cal by differential modulation of feedforward inhibitory circuits. Nature
923 communications 12(1):5475
- 924 Peng JJ, Throm B, Najafian Jazi M, et al (2023) Grid cells perform path integration in multiple reference
925 frames during self-motion-based navigation. bioRxiv pp 2023–12
- 926 Plitt MH, Giocomo LM (2021) Experience-dependent contextual codes in the hippocampus. Nature
927 neuroscience 24(5):705–714
- 928 Preuschoff K, 't Hart BM, Einhäuser W (2011) Pupil dilation signals surprise: Evidence for nora-
929 drenaline's role in decision making. Frontiers in neuroscience 5:115
- 930 Radvansky BA, Oh JY, Climer JR, et al (2021) Behavior determines the hippocampal spatial mapping
931 of a multisensory environment. Cell reports 36(5)
- 932 Ruivo LMTG, Baker KL, Conway MW, et al (2017) Coordinated acetylcholine release in prefrontal
933 cortex and hippocampus is associated with arousal and reward on distinct timescales. Cell reports
934 18(4):905–917
- 935 Sanders H, Ji D, Sasaki T, et al (2019) Temporal coding and rate remapping: Representation of nonspatial
936 information in the hippocampus. Hippocampus 29(2):111–127
- 937 Sanders H, Wilson MA, Gershman SJ (2020) Hippocampal remapping as hidden state inference. Elife
938 9:e51140
- 939 Sarel A, Finkelstein A, Las L, et al (2017) Vectorial representation of spatial goals in the hippocampus
940 of bats. Science 355(6321):176–180
- 941 Sato M, Mizuta K, Islam T, et al (2020) Distinct mechanisms of over-representation of landmarks and
942 rewards in the hippocampus. Cell reports 32(1)

- 943 Schultz W, Dayan P, Montague PR (1997) A neural substrate of prediction and reward. *Science*
944 275(5306):1593–1599
- 945 Sheffield ME, Dombeck DA (2019) Dendritic mechanisms of hippocampal place field formation. *Current*
946 *opinion in neurobiology* 54:1–11
- 947 Sheffield ME, Adoff MD, Dombeck DA (2017) Increased prevalence of calcium transients across the
948 dendritic arbor during place field formation. *Neuron* 96(2):490–504
- 949 Skaggs WE, McNaughton BL (1998) Spatial firing properties of hippocampal ca1 populations in an
950 environment containing two visually identical regions. *Journal of Neuroscience* 18(20):8455–8466
- 951 Soltani A, Izquierdo A (2019) Adaptive learning under expected and unexpected uncertainty. *Nature*
952 *Reviews Neuroscience* 20(10):635–644
- 953 Sosa M, Giocomo LM (2021) Navigating for reward. *Nature Reviews Neuroscience* 22(8):472–487
- 954 Sosa M, Plitt MH, Giocomo LM (2023) Hippocampal sequences span experience relative to rewards.
955 *bioRxiv*
- 956 Steele R, Morris R (1999) Delay-dependent impairment of a matching-to-place task with chronic and
957 intrahippocampal infusion of the nmda-antagonist d-ap5. *Hippocampus* 9(2):118–136
- 958 Sun W, Winnubst J, Natrajan M, et al (2023) Learning produces a hippocampal cognitive map in the
959 form of an orthogonalized state machine. *bioRxiv* pp 2023–08
- 960 Tanni S, De Cothi W, Barry C (2022) State transitions in the statistically stable place cell population
961 correspond to rate of perceptual change. *Current Biology* 32(16):3505–3514
- 962 Tay A (2021) Researchers are embracing visual tools to give fair credit for work on papers. *Nature Index*
963 vom 22:2021
- 964 Teles-Grilo Ruivo LM, Mellor JR (2013) Cholinergic modulation of hippocampal network function.
965 *Frontiers in synaptic neuroscience* 5:2
- 966 Tessereau C, O’Dea R, Coombes S, et al (2021) Reinforcement learning approaches to hippocampus-
967 dependent flexible spatial navigation. *Brain and Neuroscience Advances* 5:2398212820975634
- 968 Vaidya SP, Chitwood RA, Magee JC (2023) The formation of an expanding memory representation in
969 the hippocampus. *biorxiv* pp 2023–02
- 970 Vinogradova OS (2001) Hippocampus as comparator: role of the two input and two output systems of
971 the hippocampus in selection and registration of information. *Hippocampus* 11(5):578–598
- 972 Wallenstein GV, Hasselmo ME, Eichenbaum H (1998) The hippocampus as an associator of discontiguous
973 events. *Trends in neurosciences* 21(8):317–323
- 974 Williams SR, Fletcher LN (2019) A dendritic substrate for the cholinergic control of neocortical output
975 neurons. *Neuron* 101(3):486–499
- 976 Wills TJ, Lever C, Cacucci F, et al (2005) Attractor dynamics in the hippocampal representation of the
977 local environment. *Science* 308(5723):873–876
- 978 Wood ER, Dudchenko PA, Robitsek RJ, et al (2000) Hippocampal neurons encode information about
979 different types of memory episodes occurring in the same location. *Neuron* 27(3):623–633
- 980 Yu AJ, Dayan P (2005) Uncertainty, neuromodulation, and attention. *Neuron* 46(4):681–692

- 981 Zeithamova D, Gelman BD, Frank L, et al (2018) Abstract representation of prospective reward in the
982 hippocampus. *Journal of Neuroscience* 38(47):10093–10101
- 983 Zhang Y, Rózsa M, Liang Y, et al (2023) Fast and sensitive gcamp calcium indicators for imaging neural
984 populations. *Nature* 615(7954):884–891
- 985 Zinyuk L, Kubik S, Kaminsky Y, et al (2000) Understanding hippocampal activity by using purposeful
986 behavior: place navigation induces place cell discharge in both task-relevant and task-irrelevant spatial
987 reference frames. *Proceedings of the National Academy of Sciences* 97(7):3771–3776